The Curvature–Transport Correspondence (CTC) and Its Implications for Cosmic Structure Formation

Ridwan Sakidja

Dept. of Physics, Astronomy and Materials Science
Missouri State University

Abstract

This work extends the recently developed framework of the Curvature Transport Correspondence to the study of cosmic structure formation. In this framework gravitational curvature arises not from material inventories but from the divergence of a transport flux field. Mass, density, and curvature become response coefficients, much as stiffness, elasticity, and effective mass emerge in materials science from the way a medium conducts and redistributes load. This reflects a central principle of condensed matter physics: structure and rigidity are not substances but responses.

Applying this idea to three major tensions in modern physics, namely extreme cosmic inhomogeneity, the behavior of curvature inside black holes, and the large separation between the Higgs scale and the Planck scale, reveals a common origin. Each problem results from assuming that curvature is produced directly by density. Through the materials science lens of the Curvature Transport Correspondence, cosmic filaments arise from spatial variations in divergence, black hole interiors avoid singularities through flux saturation, and the hierarchy becomes a transition between soft and stiff response regimes. Taken together, these results show that many long-standing puzzles can be understood as manifestations of a single principle: curvature is the geometric response of a medium whose ability to transmit transport changes with scale.

1. Introduction: Rethinking Gravity Through the Lens of Transport

For much of modern cosmology, a single principle has guided our understanding of gravitation: *mass determines curvature*. This interpretation, rooted in Einstein's field equations, has supported the remarkable success of the ΛCDM framework. Yet as observations have sharpened, from JWST deep-field data[1] to high-resolution cosmic-web surveys[2], several persistent anomalies have begun to challenge this classical picture.

Across the observable Universe, curvature appears to respond to its environment in ways that differ from the expectations of a purely density-driven model[3]. Some regions form massive, mature galaxies far earlier than ΛCDM predicts[4]. Others evolve slowly, leaving vast voids with unexpectedly low density [5]. Structures such as filaments and walls exhibit greater coherence, length, and contrast than standard cosmology anticipates[6], [7]. These increasingly precise datasets raise a deeper question: what if curvature is not created by mass density at all, but by something more fundamental?

1.1. A Shift in Perspective

The Curvature Transport Correspondence (CTC)[8] offers an alternative formulation. Rather than interpreting the source of curvature as a static inventory of mass-energy, CTC rewrites the effective source as the divergence of a gravitational transport flux:

$$\rho_{\mathrm{eff}}(x) = \nabla \cdot F_G(x). \qquad (1\text{-}1)$$

This preserves the full mathematical structure of general relativity [9] but gives its source term a new physical interpretation. In this view curvature measures how gravitational transport flows through spacetime. When the flux converges, with the divergence negative, the result is strong collapse and rapid structure formation [10]. When the flux diverges, with the divergence positive, regions expand and voids grow [11]. When the divergence is nearly zero, the flux is balanced and the geometry evolves slowly, a pattern seen for example at the boundary of the Laniakea basin and in the saddle point regions of the cosmic web [12], [13].

This shift in perspective moves the focus from substance to flow. Curvature becomes the geometric response of spacetime to transport, not a direct reaction to mass density. The cosmological picture changes accordingly: the Universe is no longer a static inventory of material content but a dynamical system sculpted by the convergence and divergence of gravitational flux.

1.2. Why This Perspective Has Become Necessary

Several observational tensions have become too significant to ignore. Data from JWST reveal galaxies that appear far too massive and mature for their early cosmic epoch [4], [14]. Large surveys show voids and walls whose sizes and coherence are difficult to reconcile with the expectations of the standard cosmological model [15] [16] [17]. Even the Hubble tension points toward the possibility that the measured expansion rate may depend on our location within large scale inhomogeneities [18] [19]. Each of these issues could, in isolation, be attributed to astrophysical uncertainties or statistical variation. When viewed together, however, they suggest that something deeper may be amiss in our understanding of what actually sources curvature.

Within this setting the Curvature Transport Correspondence offers a different perspective. The framework leaves Einstein's equations untouched and does not require any new particles. What changes is the physical meaning of the source term. Instead of treating curvature as a response to material density, the correspondence identifies it as a response to the divergence of an underlying transport field. This shift in interpretation provides a single conceptual lens through which these diverse cosmological tensions can be understood as expressions of the same underlying mechanism.

1.3. Three Structural Tensions Motivating the CTC Framework

The Curvature Transport Correspondence is motivated by four persistent tensions in contemporary cosmology. These tensions, though traditionally treated as unrelated, share a common feature: they challenge the assumption that curvature is created directly by material density. When viewed through the lens of transport geometry, each tension appears instead as a manifestation of spatial variations or saturation in the divergence field.

<u>Extreme cosmic inhomogeneity.</u>
Large voids, highly coherent filaments, and expansive wall structures exceed the amplitude and correlation lengths predicted by the standard model. Observations of the KBC supervoid[15], the Sloan Great Wall[16], and the Hercules Corona Borealis structure[17] reveal inhomogeneities that are difficult to reconcile with Gaussian initial conditions and uniform density sourcing. In the CTC picture, such structures arise naturally from regions of strong negative or positive divergence.

Black hole singularities.
Classical general relativity predicts that curvature diverges inside black holes. This follows from the assumption that mass can collapse indefinitely. In the CTC formulation, collapse corresponds to flux convergence that is physically allowed to saturate. Singularities do not appear because the divergence field cannot grow without bound, allowing a finite curvature core to form.

The hierarchy problem.
The vast separation between the Higgs scale and the Planck scale is often interpreted as an issue of fine adjustment within the standard model. Under the CTC interpretation, this scale separation reflects a transition in how spacetime responds to divergence. Different regimes of curvature response, rather than delicate tuning of parameters, produce the observed hierarchy.

These three tensions, when considered together, reveal a pattern: they arise from the same structural assumption. They are not separate puzzles but facets of a deeper misidentification of curvature's physical source.

1.4. A view from Materials Science

From a materials-science perspective, this view arises naturally: in condensed matter physics, quantities such as stiffness[20], conductivity, and effective mass are not intrinsic substances but emergent responses to how energy, charge, and momentum flow through a material. An electron's effective mass in a crystal is not a fixed attribute; it is determined by the curvature of the electronic band structure[21]. A material's rigidity is not merely a number. Rather, it reflects how atomic bonds transmit and redistribute stress[22]. Even phase transitions are not the introduction of new ingredients but the system reorganizing its internal flows[23].

Thus, CTC asks whether spacetime behaves in the same way. What if "mass" is simply a measure of how spacetime resists bending when transport flows through it? What if cosmic voids are not passive emptiness but regions where the flow field diverges? What if the cosmological constant is not vacuum energy at all, but the faint, residual signature of an uneven transport field permeating spacetime?

This is not a leap into speculation. It is the natural extension of familiar transport principles, which is long established in materials science, to the geometry of spacetime itself.

1.5. The organization of this paper:

In the sections that follow, we examine several persistent tensions in modern cosmology and explore whether the Curvature–Transport Correspondence (CTC) might offer a clarifying perspective. While the standard ΛCDM model provides a remarkably successful framework, observations continue to reveal puzzling features. We will consider how a geometric shift in viewpoint, that is by interpreting mass and density not as fundamental substances, but as *curvature-response coefficients* emerging from transport flux, might provide a coherent, unified way of reframing these challenges:

1. Extreme cosmic inhomogeneity– Are the surprising scales of voids and filaments hints of a transport-geometric origin rather than statistical anomalies?
2. Planck–Higgs hierarchy– Could the vast scale separation reflect a vacuum stiffness transition, not a fine-tuning problem?
3. Black hole singularities– Could flux saturation prevent infinite curvature, similar to how materials saturate under extreme stress?

Our aim is not to replace established theory, but to ask: if we reinterpret the source terms in Einstein's equations geometrically, i.e. as the divergence of a gravitational transport flux, could several seemingly disconnected tensions find a common, conceptually simple explanation?

We present this exploration in the spirit of offering a complementary viewpoint, one that preserves the mathematics of GR while suggesting a shift in physical interpretation from *substance* to *transport geometry*.

2. Extreme Cosmic Inhomogeneity as a Transport-Geometry Effect

The structure of the universe tells a story of its origins, but in recent years, that story has grown unexpectedly complicated. Observations reveal a cosmic web marked by vast voids, immense filaments, and surprising coherence that pushes against the limits of standard cosmological models [2], [24]. These features challenge our understanding of how structure emerges from the smooth, uniform conditions of the early universe.

2.1. Observational Challenge

Our most precise surveys have mapped a cosmos-richer and more structured than anticipated. Consider the KBC Void[15], a spherical underdensity roughly 600 megaparsecs across, with our own Milky Way nestled near its edge. Or the immense filaments and walls revealed by galaxy surveys[6], tracing patterns across gigaparsec scales that seem improbably large and coherent. Even the scale of homogeneity, which is the distance beyond which the universe approaches uniformity[25], [26], emerges only at surprisingly large scales. Analyses of SDSS DR6 find the transition near 60–70 h^{-1} Mpc [26], while recent model-independent angular studies using S-PLUS blue galaxies identify a comparable range[25]. Together, these results indicate that the universe becomes homogeneous only at scales larger than many early theoretical models predicted, reinforcing how deeply structured the cosmic web truly is.

2.2. CTC Geometric Resolution

As introduced in Eq. (1-1), the effective source of curvature is given by the divergence of the gravitational transport flux. Spatial variations in this divergence naturally generate the observed structure of the cosmic web. Here, F_G represents a gravitational transport flux field. This simple equation reframes structure formation from a process of *matter accumulation* to one of *geometric transport organization*.
Spatial variations in this flux divergence naturally decorate the cosmic landscape:

$$\nabla \cdot F_G(x) < 0 \quad \text{(convergent flux)} \rightarrow \text{expanding voids}$$
$$\nabla \cdot F_G(x) > 0 \quad \text{(divergent flux)} \rightarrow \text{collapsing filaments and clusters}$$
$$\nabla \cdot F_G(x) \approx 0 \quad \text{(neutral flux)} \rightarrow \text{sheet-like boundaries}$$

The "sponge-like" topology of the cosmic web[10] emerges not as a statistical outlier, but as the natural equilibrium state of a transport field with spatially varying divergence.

2.3 Transport-Driven Pattern Formation

The CTC mechanism operates through a self-organizing feedback loop:

1. Initial perturbations in F_G create regions of varying divergence,
2. Divergence gradients drive curvature responses through $\rho_{\text{eff}} = \nabla \cdot F_G$,

3. Emergent curvature modifies subsequent flux evolution,
4. Self-organization produces the characteristic void-filament-sheet network.

This behavior reflects well established pattern formation dynamics in driven transport systems, where heterogeneous flux distributions evolve toward organized spatial structures such as filaments, sheets, rolls, or cellular patterns[27]. In many physical settings that involve transport and curvature operators such as divergences or Laplacians, instabilities in the flux field give rise to extended spatial organization.

Viewed in this way, the cosmic web is not only a result of gravitational instability in an expanding background but also an expression of the natural tendency of spacetime to organize transport flows. The CTC framework brings out this geometric structure clearly. Curvature and transport *do not act independently* but *coevolve* in a manner that naturally produces large scale pattern formation. CTC can potentially make specific, testable predictions that distinguish it from standard approaches:

- Void statistics: Size distributions should follow transport-divergence scaling laws rather than Gaussian random field statistics
- Morphological coherence: Filaments should exhibit greater alignment and connectivity than predicted from initial density fields alone
- Evolutionary sequence: Structure formation timing should correlate with local divergence magnitude, not just local density

In this note, it is useful to point to recent observations:

1. SDSS/BOSS surveys show filament coherence extending beyond ΛCDM expectations[28], [29].
   A very recent work by Tavasoli and Ghafour [29] shows that the observed cosmic filaments in SDSS DR10 are denser, more coherent, and structurally narrower than their ΛCDM counterparts in the IllustrisTNG300-1 simulation. The ΛCDM model can generate long macrofilaments, yet the observed Universe does not contain those same extended structures. Instead, it displays shorter but systematically denser connections. Even more striking, microfilaments linking groups and clusters show opposite trends between observation and simulation: GG filaments are denser in real data, while CC filaments are denser in ΛCDM, revealing a structural mismatch. Together, these results highlight a consistent pattern. The real cosmic web is more sharply organized and more gravitationally efficient than the ΛCDM reconstruction predicts. This tension is exactly what the Curvature Transport Correspondence can reinterpret. When curvature is based on the divergence of gravitational transport, filaments arise as self-focusing flow channels that naturally become narrower, denser, and more symmetric than the mass driven ΛCDM model allows.

2. Planck CMB lensing reveals matter distribution more structured than predicted[24]. Planck's CMB lensing analysis shows that the temperature and polarization spectra prefer a lensing amplitude higher than the ΛCDM prediction, with A_L=1.18±0.065 reported on page 3 of the Planck 2018 release. This indicates that the CMB anisotropies are more smoothed by lensing than the standard model allows, implying a matter distribution that is slightly *more clumped and more coherently organized* than predicted. Under CTC, this enhanced lensing does not require additional mass but arises naturally from stronger convergence of gravitational transport, which deepens curvature and sharpens structure.

3. DES Year 3 data indicates void properties inconsistent with Gaussian initial conditions[30].
   DES Year 3 measurements of cosmic voids show that real voids are emptier, larger, and have steeper density profiles than predicted by ΛCDM with Gaussian initial conditions. As noted in the DES

analysis, the void lensing signal is stronger than expected, and the stacked density contrast around void centers is too deep for a purely Gaussian initial field. These findings imply that matter has been evacuated from void interiors more efficiently than standard structure formation allows. In the CTC framework, such behavior arises naturally because divergence in gravitational transport amplifies flow separation, producing deeper and more coherent voids without requiring any modification to the underlying mass content.

In short, rather than representing crises for ΛCDM, these "anomalies" may reflect the underlying transport geometry of spacetime, a geometry that naturally produces large, coherent structures as it seeks equilibrium.

2.4. Materials Physics Analogy: Pattern Formation Through Transport Geometry

The geometric principles underlying CTC's explanation of cosmic structure formation find direct and well-established parallels in materials science, where similar transport mechanisms govern pattern formation across diverse physical systems. These analogs not only illuminate the CTC framework conceptually but also provide mathematical tools and scaling relationships that can be applied to cosmological structure formation.

Parallel Systems in Materials Science

Polycrystalline Grain Growth[31] offers a particularly instructive analogy. In polycrystalline materials, grain boundaries migrate according to local curvature and energy minimization principles. The divergence of grain-boundary flux determines the resulting microstructure:

- Regions of positive flux divergence become sites of void formation and interface development
- Regions of negative flux divergence experience grain growth and densification
- Neutral flux regions form stable grain boundaries that persist over extended timescales

The resulting microstructure, which is characterized by grain size distributions, boundary networks, and void arrangements, emerges directly from the geometry of grain-boundary transport rather than from random atomic arrangements. This mirrors CTC's cosmic web formation, where gravitational flux divergence determines void, filament, and sheet morphology.

Spinodal Decomposition[32] in binary alloys provides another powerful analogy. During phase separation, components separate through uphill diffusion driven by chemical potential gradients. The process follows the Cahn-Hilliard equation:

$$\frac{\partial c}{\partial t} = M\nabla^2\left(\frac{\partial f}{\partial c} - 2\kappa\nabla^2 c\right) \qquad (2\text{-}1)$$

where c is concentration, M mobility, f free energy density, and κ gradient energy coefficient. The resulting interconnected structures (typically with characteristic wavelength $\lambda \propto (\kappa/\Delta f)^{1/2}$) emerge from diffusion-flux divergence patterns, creating morphologies strikingly similar to the cosmic web's void-filament network. The statistical properties of these patterns follow universal scaling laws derived from transport geometry rather than initial concentration fluctuations.

Dislocation Patterning[33] in deformed crystals demonstrates how transport geometry shapes microstructure under external driving. Dislocations, defined as line defects in crystal lattices, organize into characteristic patterns:

- Convergent dislocation fluxes form dense deformation bands and cell walls
- Divergent dislocation fluxes create void-like channels and low-density regions
- The resulting pattern scale depends on dislocation mobility and interaction strengths

These patterns emerge from the collective dynamics of dislocation transport rather than from random defect distributions, mirroring how cosmic structure emerges from gravitational flux organization rather than random density fluctuations.

Common Principles Across Scales

These materials systems share fundamental principles with CTC's cosmological framework:

1. Transport-driven pattern formation: Structure emerges from the organization of transport fluxes rather than from static initial conditions
2. Divergence-based morphology: Positive/negative flux divergence determines void/condensation patterns
3. Scale selection: Characteristic pattern scales emerge from transport coefficients (mobility, diffusivity, interaction strengths)
4. Universal scaling: Statistical properties follow transport-determined scaling laws

This perspective transforms cosmic web formation from a unique cosmological phenomenon into a specific instance of universal transport-driven pattern formation principles operating at extreme scales. The cosmic web becomes not a statistical anomaly of random fluctuations, but the natural equilibrium structure of spacetime under heterogeneous gravitational transport. This is quite analogous to how polycrystalline microstructures represent equilibrium configurations of grain boundary transport. The convergence of cosmic and materials pattern formation principles suggests deeper connections between gravitational and condensed matter physics, potentially revealing universal laws governing pattern formation across all scales where transport processes dominate structural evolution.

3. Resolution of the Black-Hole Singularity in the Curvature–Transport Correspondence

3.1. The Singularity Problem in Classical General Relativity

Classical general relativity predicts that gravitational collapse terminates in a curvature singularity [9], [34]. For a Schwarzschild black hole, the curvature invariant that captures the full contraction of the Riemann tensor is

$$K(r) = R_{\mu\nu\rho\sigma}R^{\mu\nu\rho\sigma} = \frac{48G^2M^2}{c^4r^6}. \quad (3\text{-}1)$$

As $r \to 0$, this expression diverges,

$$\lim_{r\to 0} K(r) = \infty, \quad (3\text{-}2)$$

indicating that the geometry predicts an unbounded curvature at the central point. Because the mass $M$of the collapsing body is assumed to be concentrated into an ever-smaller volume, the implied density behaves as

$$\lim_{V\to 0} \rho_{\mathrm{GR}} = \lim_{V\to 0} \frac{M}{V} \to \infty. \ (\mathrm{V} \to 0) \qquad (3\text{-}3)$$

Thus, within the classical framework, both the energy density and the curvature invariants diverge as the collapsing matter is driven toward zero volume.

The appearance of such divergences has two implications. Mathematically, the spacetime becomes geodesically incomplete: timelike and null geodesics terminate after a finite affine parameter[35], preventing the continuation of physical trajectories beyond the central region. Physically, the theory demands the existence of infinite curvature and infinite density. These quantities that have no operational meaning and mark a breakdown in the applicability of classical general relativity.

In this sense, the Schwarzschild singularity does not represent a physical object but rather a limit of the classical equations themselves. It marks the point at which the assumption of arbitrarily compressible mass-energy becomes incompatible with a finite geometric response. This provides a natural setting in which to explore alternative formulations, such as the Curvature–Transport Correspondence, that constrain the source of curvature through physically motivated transport principles rather than through unbounded compression

3.2. CTC Perspective: From Substance to Transport

The Curvature–Transport Correspondence reframes the source of gravity. Rather than interpreting the Einstein equations as curvature sourced by a material density, the CTC approach expresses the same term as the divergence of a gravitational transport flux $F_G^{\mu\nu}$:

$$8\pi G\, T_{\mu\nu} = \nabla \cdot F_G^{\mu\nu}. \qquad (3\text{-}4)$$

In this view, gravitational collapse is not the compression of "substance" into a point but the convergence of gravitational transport:

$$\nabla \cdot F_G < 0 \text{ (convergent flux).} \qquad (3\text{-}5)$$

Singularity formation would require the transport field to converge without bound. Instead of assuming infinite compressibility of matter, the CTC framework imposes a physically motivated constraint: transport systems saturate when driven beyond their capacity.

3.3. The Flux Saturation Principle

This approach draws an analogy to a broad range of transport phenomena across physics—electronic conduction, heat flow, dislocation glide, superfluid motion—whereby saturation taken place when pushed toward extreme regimes [21], [36], [37]. Once microscopic carriers reach their maximum velocity, or once structural constraints limit further flux, the system enters a new nonlinear response regime instead of diverging. CTC extends this principle to gravitational transport:

$$\text{For } \ |F_G| \leq F_{\max}: \ |\nabla \cdot F_G| \leq D_{\max}, \qquad (3\text{-}6)$$

where $F_{\max}$ and $D_{\max}$ represent the *finite* transport capacity of spacetime. This reframes collapse entirely. Gravitational fields cannot focus indefinitely. Once the convergence reaches $|\nabla \cdot F_G| = D_{\max}$,

further compression is impossible. Collapse transitions into a saturated state, just as superfluids reorganize beyond their critical velocity or solids deform plastically beyond their yield stress.

A useful way to visualize this saturation behavior is through a mechanical analogy. Consider an acrobat riding a bicycle in a perfectly circular path. As the rider increases speed, the required centripetal force grows until the mechanical limits of the system such as the strength of the rider, the traction of the tires, and the stiffness of the frame impose a minimum turning radius. Beyond this limit, no amount of additional effort can reduce the radius any further, and the system becomes saturated. In the CTC framework spacetime behaves in the same manner. The divergence of the transport field $\nabla \cdot F_G$ determines how sharply the geometry can turn, and once this quantity reaches its maximum sustainable magnitude $D_{\max}$, curvature cannot increase further. The geometry then settles at a finite critical radius R_{crit}, inside which the divergence vanishes and the interior becomes dynamically inert. Just as a bicycle cannot trace a tighter circle once its mechanical threshold is reached, spacetime cannot support curvature below the saturation scale, and the interior remains regular instead of singular.

3.4. Mathematical Framework

The implications of the flux-saturation principle become transparent when the linearized Einstein equations are expressed within the framework of hyperbolic operators. In perturbation theory the metric is decomposed as

$$g_{\mu\nu} = \eta_{\mu\nu} + h_{\mu\nu}, \qquad (3\text{-}7)$$

and, imposing the Lorenz gauge condition

$$\partial^{\mu} \bar{h}_{\mu\nu} = 0, \bar{h}_{\mu\nu} = h_{\mu\nu} - \frac{1}{2}\eta_{\mu\nu} h, \qquad (3\text{-}8)$$

the linearized Einstein equations take the form (see Wald 1984[9]; Misner–Thorne–Wheeler 1973[38]; Maggiore 2007[39])

$$L[h_{\mu\nu}] = \nabla \cdot F_G^{\mu\nu}, \qquad (3\text{-}9)$$

where L is a second-order normally hyperbolic operator whose principal part is the wave operator $\Box$. This situates the linearized theory within the well-developed mathematical framework of hyperbolic PDEs on globally hyperbolic manifolds (Friedlander 1975[40]; Bär, Ginoux & Pfäffle 2007[41]).

Such operators admit a unique causal Green operator G, characterized abstractly by

$$L_x \, G(x, x') = \delta^{(4)}(x - x'), \qquad (3\text{-}10)$$

with support restricted to points that are causally related in the background spacetime (see Bär et al. 2007[41]; Ringström 2009[42]). No advanced distinction is required here; the operator is defined purely by linearity, hyperbolicity, and causality in the sense of normally hyperbolic operators.

Using this operator as the inverse of L, the metric perturbation admits the Green-function representation familiar from classical field theory [9], [40]:

$$h_{\mu\nu}(x) = \int_M G(x, x') \, \nabla \cdot F_G^{\mu\nu}(x') \, d^4x'. \qquad (3\text{-}11)$$

This representation follows the universal structure of solutions to linear differential equations: the Green operator encodes how a localized impulse in the divergence of the transport field at x' influences the geometry at x, and the integral reconstructs the full perturbation by superposing contributions from all points in spacetime. A key implication becomes immediate. If the transport field saturates in a region $D \subset M$ so that

$$\nabla \cdot F_G^{\mu\nu} = 0 \text{ on } D, \qquad (3\text{-}12)$$

then the Green-function integral shows that this region contributes no curvature perturbation,

$$\int_D G(x,x') \nabla \cdot F_G^{\mu\nu}(x')\, d^4x' = 0. \qquad (3\text{-}13)$$

Thus, the saturated interior is *gravitationally inert* at the level of the linearized theory: *curvature responds only to the nonvanishing divergence of the flux field outside the saturated core.* This is the geometric analogue of saturation mechanisms in electromagnetism and elasticity (e.g., conductor interiors with $\nabla \cdot E = 0$; plastically yielded regions with vanishing stress divergence).

With the assumption that the divergence of the transport flux is uniformly bounded,

$$| \nabla \cdot F_G^{\mu\nu}(x) | \leq D_{\max}. \quad (3\text{-}14)$$

Then the causal Green operator is bounded on smooth functions as well. Thus, one can obtain an estimate:

$$| h_{\mu\nu}(x) | \;\leq\; D_{\max} \int_{\mathcal{M}} | G(x,x') |\; d^4x' \;\leq\; C\, D_{\max}, \quad (3\text{-}15)$$

where C is a finite constant determined by the background geometry and gauge choice. Because curvature tensors are built from *first and second derivatives* of $h_{\mu\nu}$, any bound on $h_{\mu\nu}$ and its derivatives directly carries over to bounds on all curvature components. In the linearized regime, the wave equation ties these derivatives to the source through the Green operator, so a uniformly bounded source forces every curvature term to remain *finite*. Thus, the saturation condition of Eq. 3-14 is already sufficient to *prevent curvature from diverging*: once the divergence of the transport field cannot grow without bound, neither can the curvature it generates. This ensures that no blow-up of curvature occurs anywhere in the domain as long as the divergence remains saturated.

3.5. The Finite-Curvature Attractor

When the transport field reaches its saturation point, $\nabla \cdot F_G \to -D_{\max}$, the curvature stops growing and levels off at a constant value,

$$K \to K_{\max},\ \nabla K \to 0. \quad (3\text{-}16)$$

This means the interior region settles into a *smooth, uniform-curvature state* rather than continuing to collapse. In practical terms, the spacetime forms a stable "core" of radius r_s where the curvature no longer changes. This behavior is very similar to what is often called a de Sitter–like core in the regular black-hole literature: a calm interior region with constant positive curvature instead of a singularity.

The standard way to describe such an interior is with the familiar static, spherically symmetric metric,

$$ds^2 = -f(r)\,dt^2 + \frac{dr^2}{g(r)} + r^2 d\Omega^2, \qquad (3\text{-}17)$$

with

$$f(r) = 1 - \frac{2Gm(r)}{c^2 r}, g(r) = 1 - \frac{2Gm(r)}{c^2 r}, \quad (3\text{-}18)$$

and with a mass function that approaches a finite value near the center:

$$m(r \to 0) \to m_0 \neq 0. \quad (3\text{-}19)$$

This same overall pattern appears in many well-known non-singular black-hole models (Bardeen 1968[43]; Dymnikova 1992[44]; Hayward 2006[45]; Frolov 2016[46]): whenever the central region settles into constant curvature and maintains a finite effective mass, the interior geometry naturally takes on a de Sitter–like form. The key difference in the CTC framework is what actually *produces* this behavior. In the traditional models, the core is typically supported by vacuum energy or a de Sitter–type equation of state (Markov 1982 [47]; Frolov, Markov & Mukhanov 1990[48]), whereas in CTC the same structure emerges automatically once the gravitational transport field reaches its saturation limit and can no longer converge. In other words, the de Sitter–like core is *assumed* in the classical models but *emergent* in the CTC picture. This makes the point mass itself an emergent construct: spacetime produces it when transport saturates, rather than it being put in as a fundamental object.

Saturation halts the collapse, locks the curvature at a finite value, and produces a smooth central core instead of a singular point. In this picture, the *interior does not collapse toward an infinite-density spike*. Instead, it enters a *saturated geometric phase*. Adding more mass does not increase the curvature; it only *expands the size of the saturated region*. The curvature inside remains pinned at $K_{\max}$, which represents the transport-saturation limit of the system. The radius r_s of this core grows as additional mass is pushed into the zone where:

$$| \nabla \cdot F_G | = D_{\max}. \qquad (3\text{-}20)$$

A simple estimate for r_s follows by requiring that the interior curvature reach its saturation value

$$K(r_s) \sim K_{\max}. \qquad (3\text{-}21)$$

For a Schwarzschild like geometry, the Kretschmann scalar $K(r)$ gives the physical strength of curvature at radius r. It is the invariant that tells us how strongly spacetime is curved in a way that does not depend on coordinates. In this geometry it rises very sharply as one moves inward, and is well approximated by

$$K(r) \sim \frac{48G^2 m(r)^2}{c^4 r^6}. \qquad (3\text{-}22)$$

This expression shows two important things: curvature increases as $1/r^6$ when r becomes small, and it grows with the square of the enclosed mass. These features are the reason classical collapse produces a singularity.

In the CTC picture, *curvature cannot grow without bound*. The transport field reaches its saturation limit at $K_{\max}$, and the radius $r_s$of the saturated region is defined by the condition

$$K(r_s) = K_{\max} = \frac{48G^2 m(r_s)^2}{c^4 r_s^6} \qquad (3\text{-}23)$$

which rearranges to

$$r_s^3 \sim \sqrt{\frac{48G^2 m(r_s)^2}{c^4 K_{\max}}} \Rightarrow r_s \propto m(r_s)^{1/3}. \qquad (3\text{-}24)$$

Thus, to leading order,

$$r_s \propto M^{1/3}, \qquad (3\text{-}25)$$

which means that the radius of the *saturated core grows smoothly with the total mass enclosed*. This scaling makes the physical idea clear. Adding mass does not increase the curvature once saturation is reached. Instead, the geometry responds by enlarging the region in which curvature is already at its maximum value. The black hole interior is therefore a finite curvature region whose size reflects the total mass, while the curvature itself remains fixed at the saturation ceiling. Continued infall expands the constant curvature core rather than deepening the collapse.

3.6. Physical Interpretation: A Transport Bottleneck

Within the CTC framework, the black-hole interior behaves as a transport bottleneck.
Once the flux convergence reaches its saturation threshold, the geometry cannot support additional curvature growth. The interior responds to further infall not by deepening the collapse but by reorganizing into a larger saturated region. The physical consequences are:

- Redistribution rather than amplification:
  Additional infalling matter modifies the spatial extent of the saturated core *without* increasing curvature.
- Stabilization at the curvature ceiling:
  The curvature remains fixed at $K_{\max}$, the maximal response permitted by the transport properties of spacetime.
- Regulated collapse:
  The approach to $r = 0$ no longer represents a runaway process but a stable geometric phase.
- Mass accumulation without singularity formation:
  Increasing the mass enlarges r_s while leaving the core curvature unchanged.

In short, the core is *emergent*, not assumed: the constant-curvature interior forms on its own once flux convergence saturates, rather than being imposed through a choice of matter content.

This behavior mirrors nonlinear saturation responses encountered throughout condensed-matter physics. When a crystal reaches its yield stress or a superfluid exceeds its critical velocity, further forcing *does not produce divergence* but triggers a *structural reorganization of the medium*. In the same way, the CTC black-hole interior represents a saturated phase of spacetime, formed when the gravitational transport flux reaches its maximum convergence capacity.

3.7. Relation to Regular Black-Hole Models

Various nonsingular black hole models, for example Bardeen[43], Dymnikova[44] , Hayward[45], Frolov–Markov–Mukhanov[48], noncommutative geometry inspired constructions[49], and fuzzball proposals [49], replace the central singularity with a finite interior structure. Table 1 summarizes their regularization mechanisms and the corresponding interpretation within the CTC framework.

Table 1. Regularization mechanisms in nonsingular black hole models and their CTC interpretation

Model	Regularization mechanism	CTC interpretation
Bardeen	Effective mass function that becomes finite at the center	Flux saturation forces the mass profile to approach a finite limit $m(r) \to m_0$
Dymnikova	De Sitter like core supported by an anisotropic vacuum fluid	Constant curvature interior arises automatically once convergence reaches the saturation bound
Hayward	Curvature limiting quantum gravity correction	Geometry reaches the transport capacity limit $K \to K_{\max}$
Frolov–Markov–Mukhanov	Transition from Schwarzschild exterior to a de Sitter interior at a finite radius	Saturated region forms naturally when flux convergence cannot increase further
Noncommutative geometry models	Minimal length scale that smears the mass density	Saturation defines a natural minimal length scale r_s for the interior core
Fuzzballs	Ensemble of microstates replaces the classical interior	Microstructure interpreted as a transport domain where fine scale channels saturate

CTC reproduces the finite core behavior common to all of these regular black hole models, but grounds it in a single geometric idea rather than in model specific assumptions. The interior is the endpoint of a universal transport process. Once gravitational flux reaches its maximum convergence, the geometry enters a saturated phase with finite curvature, and the core radius expands with accumulated mass while the curvature remains fixed at its upper limit.

3.8. Numerical Simulation Framework: Curvature Saturation in a Model Black Hole Interior

To complement the analytic arguments developed in Sections 3.1–3.7, it is useful to construct a computational model that illustrates the consequences of curvature saturation in a controlled setting. The goal is not to produce a fully relativistic simulation—this lies far beyond the scope of an effective model—but rather to demonstrate, with explicit numerical solutions, how the CTC saturation principle stabilizes the curvature and generates a finite-size interior core.

The simulation adopts three structural components:

(a) Classical curvature baseline

The Kretschmann invariant for a Schwarzschild black hole is used as a reference profile,

$$K_{\mathrm{GR}}(r) = \frac{48G^2M^2}{c^4r^6}, \qquad (3\text{-}26)$$

which diverges as r^{-6} near the center. This provides a direct benchmark against which the CTC-saturated profile can be compared. Any deviation from divergence, particularly the emergence of a constant interior curvature, signals the effect of the flux saturation mechanism.

(b) CTC-inspired saturation condition

The simulation imposes an upper bound

$$K(r) \leq K_{\max}, \quad (3\text{-}27)$$

consistent with the flux saturation constraint $| \nabla \cdot F_G | \leq D_{\max}$.
The saturated core radius $r_s(M)$is defined implicitly by

$$K_{\mathrm{GR}}(r_s) = K_{\max}, \qquad (3\text{-}28)$$

giving

$$r_s(M) = \left(\frac{48G^2M^2}{c^4K_{\max}}\right)^{\frac{1}{6}}. \qquad (3\text{-}29)$$

This identifies the transition scale between the classical exterior and the finite-curvature interior. Inside r_s, the curvature is capped at $K_{\max}$, modeling the finite-curvature attractor of Sec. 3.5.

(c) Composite curvature profile

The numerical model constructs the composite function

$$K_{\mathrm{CTC}}(r) = \begin{cases} K_{\max}, r \leq r_s(M), \\ K_{\mathrm{GR}}(r), r > r_s(M), \end{cases} \qquad (3\text{-}30)$$

and compares it directly to the classical $K_{\mathrm{GR}}(r)$.
This hybrid allows for visualization of the two defining predictions of the CTC framework:

1. Emergence of a finite interior phase: curvature approaches a constant rather than diverging.
2. Mass-dependent core growth: additional mass increases r_s rather than K.

Both trends appear robustly in the numerical output.

The computational model reproduces all qualitative predictions of the analytic theory:

- Finite interior curvature: All trajectories entering the region $r \leq r_s$ encounter a constant curvature plateau rather than a divergence.
- Mass-controlled scaling: The radius of the saturated core increases approximately as $r_s \propto M^{1/3}$, consistent with the analytic expression derived from $K_{\mathrm{GR}}(r_s) = K_{\max}$.
- Smooth geometric transition: The curvature profile exhibits a continuous crossover near r_s, analogous to saturation transitions in materials systems.

- Transport bottleneck behavior: The interior curvature remains unchanged even when additional mass is added, illustrating that further collapse modifies the size, not the intensity, of the saturated region.

Although simplified, these numerical results provide a transparent demonstration of how the CTC saturation principle prevents singularity formation and produces a stable, finite-curvature interior. This simulation is *not intended* as a full solution of the Einstein equations with matter fields, nor does it rely on any particular quantum gravity formalism. Instead, it functions as a computational parable: a clear visualization of how a finite divergence field produces a finite curvature response. This aligns with the bounded-source argument in Sec. 3.4 and the conceptual picture of collapse as flux-limited transport in Sec. 3.6. Thus, the simulation serves as a numerical companion to the theoretical framework, demonstrating in explicit, reproducible terms how the Curvature–Transport Correspondence modifies the interior structure of black holes and removes the classical singularity.

3.9. Physical Interpretation of the Simulation Results

The numerical model introduced in Section 3.8 provides a transparent demonstration of the physical consequences of curvature saturation under the Curvature–Transport Correspondence (CTC). Although minimal in construction, the simulation exhibits several robust behaviors that bear directly on the interior geometry of black holes. Supplementary S2 summarize the outcomes of the Jupyter notebook.

(a) Emergence of a finite-curvature core

In the classical Schwarzschild geometry, the Kretschmann invariant diverges as r^{-6}, leading to unbounded curvature as $r \to 0$. In the CTC framework, however, the saturation of the divergence field imposes a finite ceiling $K_{\max}$. Simulation output demonstrates that:

- Curvature asymptotically approaches $K_{\max}$,
- The approach occurs smoothly as the flux convergence reaches $D_{\max}$,
- The region $r \leq r_s(M)$ becomes a constant-curvature interior phase.

This plateau is the numerical signature of the finite-curvature attractor described in Sec. 3.5.

(b) Mass accumulation increases core size, not curvature

A defining prediction of the CTC framework is that additional mass does not raise curvature indefinitely. Instead:

- The saturated curvature value $K_{\max}$remains fixed,
- The radius of the saturated core grows outward as $r_s(M) \propto M^{1/3}$.

The simulation reproduces this scaling explicitly. This behavior parallels saturation phenomena in materials systems: when a medium reaches its maximal response, further loading reorganizes the system spatially rather than intensifying the response field.

(c) Breakdown of the classical intuition of collapse

In GR, “collapse” means ever-increasing concentration of curvature. In CTC, collapse is reinterpreted as a flux process:

- The divergence $\nabla \cdot F_G$ becomes increasingly negative during collapse,
- Once it reaches $-D_{\max}$, no further convergence is possible,
- The geometry self-organizes into a finite, stable interior configuration.

The simulation shows that this transition behaves much like a phase boundary: inside the core, the curvature is pinned at $K_{\max}$; outside, the profile follows Schwarzschild scaling.

(d) The saturated interior as a transport bottleneck

The flat plateau of $K(r)$ in the simulation reflects the fact that spacetime cannot transport curvature beyond a finite capacity. This mirrors bottleneck phenomena in:

- Plastic deformation (stress saturation),
- Superfluid vortex formation (critical velocity),
- Dielectric breakdown (field saturation).

The black hole interior becomes a transport-regulated domain, not a region of runaway collapse.

(e) Implications for more complete models

Although idealized, the simulation suggests several physically meaningful consequences:

- No curvature singularity — the spacetime metric can remain smooth and geodesically complete.
- A stable interior — the saturated region behaves as a finite geometric phase.
- Observable signatures — modified ringdown spectra, echoes, and accretion dynamics may arise from this finite-curvature core.

In summary, the simulation supports the central claim of the CTC approach: singularities are replaced by saturation-driven, finite-curvature structures, consistent with both mathematical boundedness and physical analogy.

3.10 Materials Physics Analogies

The CTC resolution of black hole singularities via flux saturation finds precise and well-established parallels in condensed matter and materials physics, where similar saturation mechanisms prevent physical divergences in diverse systems [36], [37], [50]. These analogies provide not only conceptual clarity but also quantitative frameworks for understanding how spacetime responds under extreme gravitational conditions.

A. Plastic Deformation: Stress-Strain Saturation

In crystalline materials under mechanical loading, the stress-strain relationship demonstrates a clear saturation mechanism that prevents material failure through divergent deformation[37]. The process follows distinct regimes:

- Elastic regime: Stress increases linearly with strain: $\sigma = E\epsilon$, where E is Young's modulus
- Yield point: Dislocation motion initiates and dislocation flux saturates due to:
    - Forest dislocation interactions
    - Grain boundary pinning
    - Dynamic recovery mechanisms
- Plastic flow: Beyond yield, stress increases only weakly with strain: $d\sigma/d\epsilon \ll E$
- Saturation stress: Stress asymptotically approaches σ_{sat} determined by:
    - Dislocation mean free path

- Thermal activation barriers
- Microstructural constraints

Mathematically, this is often described by saturation laws such as:

$$\sigma(\epsilon) = \sigma_{\text{sat}}[1 - \exp(-E\epsilon/\sigma_{\text{sat}})]$$

or through dislocation density evolution equations:

$$\frac{d\rho}{d\epsilon} = k_1\sqrt{\rho} - k_2\rho$$

where ρ is dislocation density and k_1, k_2 are multiplication and annihilation coefficients.

CTC analog: Gravitational curvature increases with flux divergence until reaching a saturation value K_{max}, beyond which further collapse redistributes rather than intensifies curvature, similar to how plastic flow redistributes strain without catastrophic failure.

B. Dielectric Breakdown: Electric Field Saturation

In dielectric materials under high electric fields, conduction mechanisms exhibit saturation that prevents divergent current densities [36]. The phenomenon involves:

- Ohmic regime: Current density follows $J = \sigma E$ for moderate fields
- Breakdown threshold: At critical field E_{bd}, impact ionization creates charge carriers
- Avalanche saturation: Carrier multiplication saturates due to:
  - Space charge effects
  - Thermal dissipation limits
  - Material defect concentrations
- New conduction state: Material enters a high-conductivity regime without infinite current

The breakdown field often follows scaling laws:

$$E_{\text{bd}} \propto \frac{E_g^{3/2}}{\sqrt{m^*\epsilon}}$$

where E_g is band gap, m^* effective mass, and ϵ dielectric constant. Post-breakdown, the current-voltage characteristic saturates:

$$J(E) = J_{\text{sat}}\left[1 + \left(\frac{E}{E_0}\right)^n\right]^{\frac{1}{n}}$$

with saturation current J_{sat} determined by carrier mobility and recombination rates.

CTC analog: Spacetime reaches a maximum curvature response at critical flux divergence D_{max}, analogous to dielectric breakdown field. Beyond this, gravitational transport continues but without producing divergent curvature, just as current continues without infinite density after dielectric breakdown.

C. Superfluid Critical Velocity: Flow Saturation

In superfluid, the onset of dissipation occurs at a critical velocity v_c rather than through divergent resistance [50]. The Landau criterion establishes:

$$v_c = \min_p \frac{E(p)}{p}$$

where $E(p)$ is excitation energy spectrum. Above v_c:

- Vortex nucleation: Quantized vortices form, carrying circulation $\kappa = h/m$
- Vortex tangle development: Vortices interact and form complex networks
- Mutual friction: Vortex-phonon interactions dissipate energy
- Saturated dissipation: Additional velocity increase produces proportionally **more vortices** rather than divergent friction

The relationship between superflow velocity v_s and vortex line density L follows:

$$\frac{dL}{dt} = \alpha v_s L^{3/2} - \beta L^2$$

where α and β are creation and annihilation coefficients. In steady state:

$$L \propto (v_s - v_c)^2$$

The critical velocity thus represents a saturation threshold beyond which additional forcing increases vortex density rather than producing divergent dissipation.

CTC analog: Gravitational transport saturates at critical divergence D_{max}, analogous to superfluid critical velocity. Beyond this, additional collapse produces geometric reorganization (e.g., changes in internal black hole structure) rather than divergent curvature.

Common Mathematical Structure

These diverse saturation behaviors follow a shared mathematical pattern. A broad set of systems can be modeled by evolution equations of the form

$$\frac{dX}{dt} = \alpha\, X^m\, (1 - \frac{X}{X_{\text{sat}}})^n - \beta\, X^p,$$

where $X$is the evolving quantity, $X_{\text{sat}}$is the saturation value, and the exponents m, n, preflect the underlying physics. The first term represents growth or multiplication, amplified by the current value of X. The factor

$$\left(1 - \frac{X}{X_{\text{sat}}}\right)^n$$

introduces nonlinear saturation, directly paralleling the generalized logistic (Richards) growth law[51], where growth slows as a system approaches its carrying capacity. The second term, βX^p, plays the role of a recovery or annihilation process that removes the quantity as it accumulates.

This structure has a wide range of applications:

- In materials science, it mirrors the Kocks–Mecking dislocation evolution law[52], where dislocations multiply through storage mechanisms and saturate through dynamic recovery, following:

$$\frac{d\rho}{d\varepsilon} = k_1\rho^{1/2} - k_2\rho,$$

which is exactly a generation term − annihilation term with, in this case, exponents $m = \frac{1}{2}$ and $p = 1$, leading to saturation of ρ with strain.

- In nonlinear transport systems (carrier recombination, vortex dynamics, curvature evolution), the same competition between nonlinear growth and annihilation produces a stable limiting value[27], [53], [54].

Across these very different physical contexts, the same mathematical logic appears: saturation is the emergent balance between a growth channel that increases X and a nonlinear mechanism that progressively limits or removes it.

3.11. Implications for Black Hole Physics

The saturation mechanisms seen in materials systems provide a useful template for understanding how curvature may behave inside black holes. If spacetime possesses a finite transport capacity, analogous to the finite defect, carrier, or vortex capacities of condensed-matter systems, then several structural consequences naturally follow:

- Saturation scaling:
  Curvature should approach a finite upper value $K_{\max}$, with an interior profile of the form

$$K(r) = K_{\max}\,[1 - f(r)],$$

where $f(r) \to 0$ as $r \to 0$. Instead of diverging, curvature asymptotically approaches a maximum set by the transport limits of spacetime.

- Critical behavior:
  Near the saturation threshold, curvature can exhibit scaling laws similar to those in nonlinear saturation systems:

$$K_{\max} - K(r) \sim r^{\delta},$$

where δ depends on the specific transport geometry and the nonlinear response of F_G.

- Internal structure formation:
  A saturated interior is not featureless. Finite-capacity systems—such as crystals near dislocation saturation or superfluids near vortex saturation—often reorganize into cell-like substructures or tangled configurations. Analogously, the black hole core may contain geometric microstructure dictated by the saturation of curvature.
- Energy dissipation and reorganization:
  Approaching $K_{\max}$likely involves a redistribution of flux or curvature analogous to defect

rearrangement in materials. This geometric reorganization would dissipate gravitational energy and stabilize the interior.

This perspective transforms singularities from inevitable mathematical consequences of GR to artifacts of an oversimplified constitutive relation—one that assumes linear response continues indefinitely. In reality, as in materials, extreme conditions reveal nonlinear saturation behavior that preserves finiteness while allowing continued evolution.

The parallel with plastic deformation, dielectric breakdown, and superfluid critical velocity provides not only conceptual support for CTC's approach but also a rich mathematical framework for developing detailed models of black hole interiors, potentially bridging the gap between classical GR descriptions and anticipated quantum gravity corrections.

3.12. From Singularity to Saturation

In traditional GR, singularities arise because the source term is treated as if matter can be compressed indefinitely. The Curvature–Transport Correspondence reframes this: spacetime has finite transport capacity, so curvature cannot grow without bound. Singularities are therefore not physical objects but artifacts of assuming that a linear constitutive relation remains valid under arbitrarily extreme conditions.

Under CTC, the interior of a black hole behaves much like a material driven beyond its linear-response regime. Materials do not support infinite stress; they *yield*[52]. Dielectrics do not sustain infinite electric field; they *break down*[55]. Superfluids cannot exceed their critical velocities; they *nucleate vortices*[54]. In each case, nonlinear saturation mechanisms intervene to preserve finiteness.

Likewise, spacetime resists infinite curvature. Once the transport capacity is approached, the system shifts into a nonlinear, saturating regime that limits curvature to $K_{\max}$while still allowing continued evolution of the geometry. The result is a regular, structured interior rather than a pathological singularity.

This perspective turns black hole singularities from unavoidable predictions into signs of an *incomplete constitutive model*. By importing intuition and mathematics from materials science, where saturation, reorganization, and finite response capacities are foundational, we obtain not only a physically grounded resolution mechanism but also a framework for constructing detailed interior models. Such models may naturally connect classical GR with the scales where quantum gravity sets the ultimate bound $D_{\max}$, providing a bridge rather than a discontinuity between the two regimes.

3.13. Jet Emission as a Test of the Saturated-Core Framework

Once the saturated interior forms the transport field collapses inside a finite radius, creating a region where $F_G = 0$and gravitational flux cannot be carried inward. All subsequent mass-energy must reorganize around this saturation boundary rather than penetrate the interior. This structural constraint places a strict limit on how deeply magnetic fields can be compressed and how much curvature amplification the system can support. As a result the mechanism that ordinarily powers relativistic jets enters a fixed-output, saturation-limited regime.

In general relativity jet power is expected to rise steeply with black hole mass because magnetic flux can be advected arbitrarily close to the center, allowing curvature and frame dragging to strengthen without internal constraints. This leads to the familiar scaling

$$P_{\mathrm{GR}} \propto M^2.$$

Under the Curvature–Transport Correspondence this behavior cannot persist once a saturated core has formed. With the interior unable to carry additional transport, the boundary at R_{crit}determines the maximum magnetic compression the system can sustain. Jet power therefore becomes limited by the structure of this boundary rather than by the mass of the object. The jet enters a saturation plateau, characterized by

$P_{\mathrm{CTC}} \approx P_{\mathrm{sat}}$ for objects that retain a saturated interior.

Here P_{CTC} denotes the jet power predicted by the transport-based model, M_{eff} is the effective gravitational mass determined by the divergence of the flux field outside the saturated core, and $M_{\mathrm{sat}}$is the saturation mass corresponding to the largest effective mass the saturated configuration can support before inward transport reactivates. Once a saturated core exists, variations in accretion rate or inflowing mass do not translate into stronger jets: the interior cannot respond, the boundary does not shift, and the jet-launching region operates at a fixed transport capacity. Only when the accumulated effective mass approaches M_{sat}can the saturated configuration destabilize, allowing renewed inward transport and a departure from the plateau. Until this point the system is mass-blind—jet power reflects the saturated boundary rather than the instantaneous mass inflow.

A flattening of jet luminosity is already seen across several astrophysical populations. X-ray binaries, spanning nearly an order of magnitude in mass, exhibit fairly identical jet powers in their low/hard states, deviating strongly from the GR scaling [56], [57]. Low-luminosity active galactic nuclei show the same trend: their jet luminosities vary only weakly with mass, following a shallow dependence far below the GR expectation [58], [59]. Even the Milky Way centre, where GR predicts a powerful jet from its four-million-solar-mass black hole, is anomalously quiet and lies on the same mass-independent locus[60].

Even in tidal disruption events, where a sudden increase in accretion should dramatically amplify jet power, observed jet luminosities remain comparable to those from stellar mass systems. Bloom et al. (2011) report a relativistic jet from a 10^6–$10^7 M_\odot$ black hole whose power is far smaller than the GR scaling $P \propto M^2$ would predict and instead lies on the same mass independent jet locus seen in X-ray binaries and low luminosity AGN.

Tidal disruption events offer a clean opportunity to test jet–mass scaling because the central black hole is normally quiescent before the flare and the jet is newly formed. The transient Swift J1644+57 provides the strongest case. Bloom et al. (2011) [61] first identified the event as a relativistic outburst powered by a sudden accretion episode onto a black hole of mass $10^6 - 10^7\ M_\odot$, and Zauderer et al. (2011) [62] subsequently demonstrated through radio and VLBI observations that the source launched a mildly relativistic, highly collimated jet with a broadband synchrotron spectrum. Remarkably, the jet power inferred from both analyses is comparable to that of the most powerful stellar-mass microquasars rather than scaling as M^2 as general relativity predicts. Even after correcting for beaming, the intrinsic energetics remain near the Eddington luminosity of a $10^6\ M_\odot$ black hole, placing Swift J1644+57 on the same mass-independent jet locus as X-ray binaries and low-luminosity AGN. GR offers no internal

mechanism to suppress the mass dependence of jet power in such systems, but in the CTC framework this behavior arises naturally: once the interior transport field saturates and $F_G = 0$ inside the critical radius, magnetic flux cannot be further compressed and the jet becomes limited by the fixed transport capacity of the saturation boundary rather than by the black hole mass. Thus, Swift J1644+57 serves as a direct observational example of a million-solar-mass system producing a jet at the universal saturation plateau expected from a saturated-core spacetime.

These observations altogether supports a universal plateau in jet power across systems that differ in mass by up to eight orders of magnitude. In the CTC framework this behavior arises naturally. Once the interior flux collapses and $F_G = 0$ inside the critical radius, spacetime can no longer compress magnetic fields or amplify curvature. The jet mechanism reaches a finite ceiling, yielding a mass-independent jet power for all systems with $M_{\rm eff} < M_{\rm sat}$. General relativity has no internal saturation scale and therefore cannot generate this plateau without substantial fine tuning of accretion or environmental conditions.

This yields a clear, falsifiable prediction. If future observations show no evidence of saturation and instead confirm the mass-squared scaling across all environments, the CTC model must be revised. If the observed plateau persists in weakly accreting systems, the transport interpretation gains significant support. Jet emission therefore provides a direct probe of the constitutive behavior of spacetime and an empirical path for testing the CTC with current and next-generation high-resolution data.

4. The Mass Hierarchy as a Rigidity Gap in the Vacuum

4.1. The Traditional Hierarchy Problem

The enormous separation between the electroweak and Planck scales represents one of particle physics' most persistent puzzles [63], [64]:

$$\frac{M_{\rm Pl}}{v_{\rm EW}} \approx \frac{1.22\times10^{19}\ \text{GeV}}{246\ \text{GeV}} \approx 5 \times 10^{16} \quad (4\text{-}1)$$

where $v_{\rm EW}$ is the Higgs vacuum expectation value. In the Standard Model, quantum corrections to the Higgs mass are quadratically sensitive to the cutoff scale:

$$\Delta m_H^2 \sim \frac{\Lambda_{\rm UV}^2}{16\pi^2} \quad (4\text{-}2)$$

For $\Lambda_{\rm UV} \sim M_{\rm Pl}$, this yields corrections $\sim 10^{30}$ larger than the observed $m_H \approx 125$ GeV[65]. The required cancellations to ~ 1 part in 10^{28} constitute the "naturalness problem" [66], traditionally motivating supersymmetry, composite Higgs models, or other new physics at the TeV scale [67].

4.2. CTC Resolution: Vacuum Stiffness Spectrum

The Curvature–Transport Correspondence reinterprets this hierarchy not as a fine-tuning problem, but as a geometric stiffness transition in the vacuum's curvature response. In CTC, mass emerges as a curvature-response coefficient:

$$m_{\rm eff} \propto \left(\frac{d^2E}{dk^2}\right)^{-1} \text{ for field excitations} \quad (4\text{-}3)$$

This relationship reveals that what we measure as "particle mass" quantifies the *vacuum's resistance to field curvature*. Different energy scales correspond to *different vacuum rigidity regimes*.

4.3 Vacuum Rigidity Spectrum

The CTC framework proposes a continuous stiffness spectrum for the vacuum:

A. Planck Regime ($E \gtrsim M_{\text{Pl}}$): Ultra-Rigid Phase

$$\kappa_P \sim M_{\text{Pl}}^4 \text{ (Planckian bending modulus)} \quad (4\text{-}4)$$

- Characteristics: Near-infinite resistance to curvature, minimal field fluctuations
- Mechanism: Quantum gravitational effects enforce maximal stiffness due to its massive intrinsic energy density, which would be extremely "rigid" gravitationally [68]
- Consequence: Particle-like excitations cannot form; spacetime behaves as an effectively rigid medium

B. Intermediate Regime ($v_{\text{EW}} \lesssim E \ll M_{\text{Pl}}$): Rigidity Gap

$$\kappa_{\text{gap}} \gg \kappa_{\text{Higgs}} \quad (4\text{-}5)$$

- Characteristics: Strong resistance persists but begins to soften
- Observation: No known particles in this range (10^4–10^{18} GeV) [69]
- Interpretation: Insufficient vacuum compliance to support resonant excitations

C. Higgs Regime ($E \sim v_{\text{EW}}$): Compliant Phase

$$\kappa_H \sim v_{\text{EW}}^4 \quad (4\text{-}6)$$

- Characteristics: Vacuum becomes sufficiently flexible to support curvature
- Mechanism: Electroweak symmetry breaking reduces vacuum stiffness [70]
- Consequence: Higgs boson and massive gauge bosons emerge as curvature resonances

D. QCD Regime ($E \lesssim \Lambda_{\text{QCD}} \approx 200MeV$): Soft Phase

$$\kappa_{\text{QCD}} \ll \kappa_H \quad (4\text{-}7)$$

- Characteristics: Highly compliant vacuum enables strong curvature
- Manifestation: Confinement, chiral symmetry breaking (CSB), hadron masses [71]
- Result: 99% of visible mass emerges from QCD curvature response

4.4. Stiffness Scale Relation

Within the Curvature Transport Correspondence, the vacuum stiffness $\kappa(E)$ measures the resistance of spacetime to curvature sourced by the effective density $\rho_{\text{eff}} = \nabla \cdot F_G$. Because curvature in this framework is generated by transport rather than static mass density, $\kappa(E)$ must vary across energy scales. Scale dependent response coefficients of this type are well known in condensed matter and materials science [20], [21], [72], [73], where moduli, conductivities, and effective masses evolve according to the reorganization of microscopic transport channels. A closely related structure appears in the scaling theory of localization developed by Abrahams, Anderson, Licciardello, and Ramakrishnan

[74], where the conductivity σ satisfies a similar inverse susceptibility flow equation. These analogies are summarized in Supplementary Note S2.

Motivated by this correspondence, the running of vacuum stiffness is expressed in transport form:

$$\frac{d\kappa(E)}{dE} = -\frac{\kappa(E)}{\gamma(E)}, \qquad (4\text{-}8)$$

where $\gamma(E)$ is a stiffness susceptibility capturing the ease with which the geometric transport network redistributes flux. Separating variables,

$$\frac{d\kappa}{\kappa} = -\frac{dE}{\gamma(E)}. \qquad (4\text{-}9)$$

Integrating from the electroweak scale v_{EW} to a general energy E,

$$\ln\left[\frac{\kappa(E)}{\kappa(v_{EW})}\right] = -\int_{v_{EW}}^{E} \frac{dE'}{\gamma(E')}. \qquad (4\text{-}10)$$

The stiffness–scale relation can then be viewed as:

$$\kappa(E) = \kappa(v_{EW}) \exp\left[-\int_{v_{EW}}^{E} \frac{dE'}{\gamma(E')}\right]. \qquad (4\text{-}11)$$

The key feature is the behavior of $\gamma(E)$ *near the Planck regime*. As E approaches M_{Pl}, the density of geometric microstates increases extremely rapidly, a fact well established in semiclassical quantum gravity and in the statistical interpretation of black hole entropy [75], [76]. In this limit the inverse susceptibility behaves proportionally to the derivative of the Bekenstein-Hawking entropy with respect to energy,

$$\frac{1}{\gamma(E)} \sim \frac{dS_{BH}}{dE}, E \to M_{Pl}, \qquad (4\text{-}12)$$

since each increment in energy accesses an exponentially large number of horizon microstates.

Accordingly,

$$\int_{v_{EW}}^{M_{Pl}} \frac{dE'}{\gamma(E')} \approx S_{BH}, \qquad (4\text{-}13)$$

capturing the *cumulative entropy cost of reorganizing geometric transport between the electroweak and Planck scales*. Substituting this result into (4.14), one obtains

$$\kappa(M_{Pl}) = \kappa(v_{EW}) exp\,[S_{BH}]. \qquad (4\text{-}14)$$

The exponential hierarchy between electroweak and Planck stiffness thus arises *naturally* within the CTC framework. No fine tuning is required. The hierarchy reflects the intrinsic transport structure of spacetime and the vast entropy associated with Planck scale microstates. The familiar problem of stabilizing the electroweak–Planck hierarchy becomes an emergent consequence of transport driven curvature dynamics rather than an anomaly of particle masses.

4.5. Connection to Effective Field Theory

A natural way to express the influence of the Curvature–Transport Correspondence on matter fields is through the structure of the effective Lagrangian. For a generic scalar sector, the low-energy action can be written schematically as

$$\mathcal{L}_{\text{eff}} = \mathcal{L}_{\text{kin}} + \frac{1}{\kappa(E)}(\partial\phi)^2 + V(\phi). \qquad (4\text{-}15)$$

This form is entirely standard in effective field theory: the coefficient multiplying the kinetic term plays the role of a scale-dependent wavefunction normalization factor, conventionally denoted $Z(E)$. In the CTC framework we identify

$$Z(E) = \frac{1}{\kappa(E)}. \qquad (4\text{-}16)$$

The mathematics is conventional; the unique perspective in this case lies in the physical origin of $Z(E)$. In ordinary EFT, the running of the kinetic coefficient is induced by quantum fluctuations of the fields. In the CTC picture, the running instead reflects the transport properties of spacetime, encoded in the vacuum stiffness $\kappa(E)$. The evolution of this stiffness is governed by the flow equation

$$\frac{d\kappa(E)}{dE} = -\frac{\kappa(E)}{\gamma(E)}, \qquad (4\text{-}17)$$

where $\gamma(E)$is the transport susceptibility. This differential equation is separable:

$$\frac{d\kappa}{\kappa} = -\frac{dE}{\gamma(E)}. \qquad (4\text{-}18)$$

Integrating between two scales $E_0$and E:

$$\ln\left[\frac{\kappa(E)}{\kappa(E_0)}\right] = -\int_{E_0}^{E} \frac{dE'}{\gamma(E')}, \qquad (4\text{-}19)$$

and exponentiating gives the explicit stiffness flow

$$\kappa(E) = \kappa(E_0)\exp\left[-\int_{E_0}^{E} \frac{dE'}{\gamma(E')}\right]. \qquad (4\text{-}20)$$

This shows that $\kappa(E)$changes *exponentially* with energy scale whenever the susceptibility $\gamma(E)$becomes small, particularly near the Planck regime. The running of the kinetic term is therefore

$$Z(E) = \frac{1}{\kappa(E_0)}\exp\left[\int_{E_0}^{E} \frac{dE'}{\gamma(E')}\right]. \qquad (4\text{-}21)$$

Extraction of Physical Mass

In a canonically normalized theory, the physical mass satisfies

$$m_{\text{phys}}^2 = \frac{m_0^2}{Z(E)}. \qquad (4\text{-}22)$$

Using $Z(E) = 1/\kappa(E)$:

$$m_{\text{phys}}^2 = m_0^2\, \kappa(E). \qquad (4\text{-}23)$$

Substituting the CTC stiffness flow:

$$m_{\text{phys}}^2(E) = m_0^2\, \kappa(E_0) \exp\ \left[-\int_{E_0}^{E} \frac{dE'}{\gamma(E')}\right]. \qquad (4\text{-}24)$$

This makes the hierarchy mechanism explicit: if $\gamma(E)$ becomes small near $E \sim M_{\text{Pl}}$, the integral becomes large, and the physical mass at low energy becomes exponentially suppressed. Thus

$$m_{\text{phys}}(v_{\text{EW}}) \ll m_{\text{phys}}(M_{\text{Pl}}), \qquad (4\text{-}25)$$

without any fine tuning of the potential $V(\phi)$or delicate cancellations in the Standard Model.

Implication

Large separations between physical scales arise from geometric renormalization: the exponential flow of the vacuum stiffness as the universe cools from the Planck era to electroweak energies. The EFT formulation does not modify Standard Model fields or interactions; it simply incorporates the fact that the geometric background is a transport medium with a scale-dependent stiffness. In this way, the CTC fits naturally into the language of effective field theory while providing a distinctive, first-principles mechanism for generating physical hierarchies.

5.6. Materials Physics Analogy: Mechanical Phase Transitions

The CTC framework's interpretation of the Planck–Higgs hierarchy as a vacuum stiffness transition finds compelling, well-established parallels in materials systems where mechanical properties change abruptly due to underlying structural transitions. These analogies not only offer conceptual clarity but also provide a robust physical and mathematical foundation for understanding how dramatic property changes can emerge naturally from the geometry of the underlying medium.

Jamming Transitions in granular materials [77] illustrate how mechanical stiffness can vary over orders of magnitude with only minor changes in packing density. At low densities, grains flow like a fluid with minimal rigidity. As density increases toward the jamming point ϕ_J, the system undergoes a continuous but sharp transition: the bulk and shear moduli rise from near zero to finite values, and the material becomes solid. This transition is not controlled by tuning microscopic parameters but emerges from geometric constraints and contact network formation. The scaling of elastic moduli near the jamming point follows power laws:

$$G, K \sim (\phi - \phi_J)^{\alpha} \qquad (4\text{-}26)$$

where exponents α are universal across many disordered systems. Crucially, the dramatic change in stiffness occurs without any change in the intrinsic properties of the grains—only their packing geometry. In the CTC view, the vacuum near the Planck scale may be in a "jammed" state where geometric constraints naturally enforce extreme rigidity.

Glass Transitions in supercooled liquids [78] demonstrate how kinetic and mechanical properties can change by many orders of magnitude across a narrow temperature range without an underlying thermodynamic singularity. As a liquid is cooled below its melting point, its viscosity η increases dramatically, often following the Vogel–Fulcher–Tammann law:

$$\eta(T) \sim \eta_0 \exp\left(\frac{A}{T-T_0}\right) \quad (4\text{-}27)$$

where T_0 is the ideal glass transition temperature. Near T_g, relaxation times increase from picoseconds to centuries, and the shear modulus rises from near-zero to values typical of solids. This "fragile-to-strong" transition reflects a growing correlation length in dynamical heterogeneity, not a change in molecular interactions. Analogously, CTC proposes that the vacuum's "relaxation time" to curvature perturbations changes dramatically across the Planck–Higgs energy gap due to evolving dynamical correlations in the gravitational flux field.

Quantum Critical Points[23] provide a third powerful analogy, where stiffness can diverge as a system approaches a zero-temperature phase transition tuned by a non-thermal parameter (pressure, magnetic field, or chemical doping). Near quantum criticality, the elastic modulus or sound velocity can show power-law scaling:

$$c_s \sim | g - g_c |^{\nu z} \quad (4\text{-}28)$$

where g is the tuning parameter, g_c the critical point, and ν, z critical exponents. In some quantum magnets or heavy-fermion systems, the spin-stiffness changes by orders of magnitude near the quantum critical point. This divergence reflects the softening of a collective mode and the growth of quantum fluctuations—precisely the kind of behavior CTC suggests may characterize the vacuum's response near the Planck scale, where quantum gravitational fluctuations become dominant.

Thus, the immense gap between the Higgs mass scale and the Planck scale (the hierarchy problem) might not be a problem of missing particles, but rather the result of this very power-law scaling across a transition region. The "stiffness" of the vacuum drops off dramatically, following a power law, as energy scales decrease, naturally explaining the vast differences in fundamental force strengths we observe.

Common Principles: Emergence Without Fine-Tuning

These materials transitions share several key features with the CTC interpretation of the hierarchy problem:

1. Abrupt property changes without microscopic tuning: Large changes in macroscopic stiffness arise from collective reorganization, not from adjusting microscopic parameters.
2. Universality and scaling: Critical exponents and scaling functions are often independent of microscopic details, suggesting that the hierarchy's scale ratio may be universal rather than finely tuned.

3. Geometric or topological origin: In jamming and glass transitions, the changes stem from geometric constraints and growing correlation lengths, not from changes in fundamental constants.
4. Separation of scales: The transition region (in density, temperature, or field) is narrow compared to the range of property variation, mirroring the narrow energy window between the Higgs and Planck scales compared to their ratio.

5.8. Vacuum Stiffness as a Scale-Dependent Response

In the CTC framework the vacuum is not treated as a medium with fixed elastic properties, but as a system whose effective stiffness changes with energy scale. This mirrors familiar behavior in materials science, where rigidity is not intrinsic but emerges from how microscopic degrees of freedom reorganize under load. Polymers stiffen when stretched, foams stiffen upon compression, glasses develop scale-dependent rigidity near jamming, and quantum critical systems show emergent elastic responses when tuned through a transition.

Guided by these analogies, we describe the vacuum stiffness as a scale-dependent response function,

$$\kappa(E) = \kappa_0 \, F\left(\frac{E - E_t}{\Delta E}\right),$$

where E_t marks the energy at which the vacuum changes behavior, ΔEsets the width of the crossover region, and $F(x)$ is a scaling function analogous to those used in rigidity percolation, jamming, or quantum critical scaling.

The essential point is that $\kappa(E)$is not constant. It is an emergent property determined by which degrees of freedom are active at a given scale and how efficiently they transmit or resist curvature. If the vacuum enters a stiff phase above a transition energy of order the Planck scale, its behaviour can be approximated by a scaling relation,

$$\kappa(E) \sim \kappa_0 (\frac{E - E_t}{\Delta E})^{\beta}, E \gtrsim E_t,$$

where a positive exponent βcharacterizes the onset of stiffness. A different exponent would describe the soft regime associated with electroweak symmetry breaking below the transition.

This perspective reframes the enormous hierarchy between the electroweak and Planck scales. Instead of requiring delicate cancellations among fundamental parameters, the hierarchy arises naturally from a shift in the vacuum's rigidity as the energy scale crosses E_t. In standard field theoretic language this appears as a dramatic change in the effective mass scale; in the CTC language it corresponds to a change in the vacuum's ability to resist curvature or support transport convergence.

The Higgs sector thus probes a soft phase of the vacuum, while gravitational processes near the Planck scale probe a stiff phase. The hierarchy reflects the scaling behavior of $\kappa(E)$, not fine-tuning in the Lagrangian. In the CTC picture curvature is a response to the divergence of a transport field, and $\kappa(E)$ determines how strongly curvature responds to a given flux configuration. As a result:

- in the *soft regime***,** curvature responds gently and the effective mass scale is low
- in the *stiff regime*, curvature responds strongly and saturates quickly, preventing singularities

The scale-dependent stiffness thus unifies two seemingly disparate contexts: the soft regime relevant for particle physics and the stiff regime that caps curvature in gravitational collapse.

5.9. Connection to Quantum Field Theory: Vacuum Response and the Scaling Gap

The discussion of vacuum stiffness can be understood without relying on materials analogies. The basic idea already appears in quantum field theory. In QFT the vacuum is not empty; it is a condensate that reacts when fields try to deform it. The Higgs mechanism makes this explicit: particles gain mass because the vacuum resists their motion. In this sense, the Higgs condensate acts like a low-energy stiffness of the vacuum. However, standard QFT is built on flat spacetime, so this vacuum response is never treated as something that could influence geometry. QFT can explain how mass emerges, but not how that same vacuum response might affect curvature. Because of this limitation, the huge gap between the Higgs scale and the Planck scale appears mysterious.

The CTC framework resolves this. If vacuum stiffness is viewed as a transport property of spacetime itself, then the jump between the Higgs scale and the Planck scale becomes a *natural crossover between two phases of the vacuum*. At low energies the vacuum is soft and easy to deform. Near the Planck scale it becomes extremely stiff and strongly resists flux convergence. The hierarchy is simply the energy window over which this change happens. In QFT terms it is the range where the vacuum's response function shifts from very weak to very strong.

This closes the conceptual gap between QFT and GR. The mechanism that gives particles mass and the mechanism that limits curvature become two expressions of the same underlying phenomenon: the way *the vacuum transmits gravitational transport.* The Higgs condensate represents the soft phase of this vacuum, while the Planck regime represents the stiff phase where curvature saturates.
Seen this way, the hierarchy problem *does not require new particles or added symmetries*. It follows from the vacuum's own behavior. As the energy increases, the vacuum's stiffness changes, and this change naturally separates the electroweak and Planck scales. Mass, curvature, and the hierarchy all arise from a single idea: *the vacuum's energy-dependent ability to carry gravitational flux.*

6. Unified Summary: Three Problems, One Underlying Principle

Viewed through the combined lens of the Curvature–Transport Correspondence (CTC) and materials-science intuition, three puzzles that normally live in separate corners of physics begin to fall into the same pattern. The unexpectedly strong inhomogeneities of the cosmic web, the question of what happens to curvature inside black holes, and the vast gap between the Higgs and Planck scales all look very different on the surface. Yet once curvature is understood as a response to the divergence of a transport field—much like stress or stiffness emerging from how a material conducts load—they reveal a shared origin. In each case, the essential physics comes down to how the vacuum transmits, concentrates, or saturates gravitational flux, and how that transmission changes with scale.

Cosmic Structure

Variations in flux divergence naturally generate the observed filament–void network and place bounds on the amplitude and coherence of large-scale inhomogeneities. Regions where flux concentrates reach saturation, limiting curvature growth and producing the characteristic patterns seen in surveys.

Black-Hole Interiors

As gravitational collapse intensifies, flux convergence hits its intrinsic limit. Curvature saturates, a finite-radius core forms, and the interior settles into a stable, constant-curvature phase. This removes the classical singularity and yields an interior whose size grows with mass while curvature remains bounded.

The Hierarchy / Scaling Gap

At low energies the vacuum behaves as a soft medium, and QFT excitations deform it easily, producing the electroweak scale. At high energies the vacuum becomes stiff, transmitting flux with increasing resistance until curvature saturates at the Planck scale. The hierarchy is then the crossover between these two phases, not a fine-tuning problem.

Taken together, these three cases show that problems normally treated as unrelated all arise from a common geometric response property of the vacuum. In this sense, CTC replaces a collection of isolated puzzles with a unified picture: mass, curvature, structure formation, and scaling all reflect how the vacuum conducts and redistributes gravitational transport across energy scales.

7. Conclusion

The curvature–transport correspondence reframes gravity in a simple but powerful way: curvature is not sourced by material densities, but by the divergence of a gravitational transport field. With this shift in interpretation, several long-standing tensions in modern physics fall into a unified pattern. The large inhomogeneities of the cosmic web, the emergence of finite-curvature cores inside black holes, and the hierarchy between the Higgs and Planck scales all arise naturally once spacetime is viewed as a medium whose ability to transmit gravitational flux varies with scale.

No modification of general relativity is required. What changes is the physical meaning of the source term: density and mass become emergent response properties, much like stiffness or rigidity in complex materials. In this picture, cosmic structure, black-hole interiors, and particle-physics mass scales are different manifestations of the same underlying behavior—how the vacuum channels, concentrates, and ultimately saturates gravitational transport. By grounding curvature in transport rather than substance, the CTC framework offers a unified geometric account of phenomena across an enormous range of scales. Instead of calling for exotic new ingredients, the Universe's apparent anomalies become signatures of a single organizing principle that has been present all along.

Acknowledgement

I acknowledge the support of the Matthew & Patricia Harthcock Fellowship from the College of Natural and Applied Sciences (CNAS), Missouri State University**,** which provided the time and resources necessary for this work. I am deeply grateful to my family, whose encouragement has sustained this project, and to my colleagues and students, whose engagement and thoughtful discussions continually strengthened the ideas developed here. I also note that large language model (LLM) tools were used in preparing this manuscript, particularly for clarifying conceptual arguments and assisting with code development. The ideas, derivations, and scientific conclusions, however, are solely the responsibility of the author.

The Jupyter and Python scripts used to generate the figures and numerical examples in this work are freely available, together with the preprint, in the GitHub collection CTC_related_papers**:** https://github.com/sakidja/CTC_related_papers

REFERENCES

[1] J. P. Gardner *et al.*, "The James Webb Space Telescope Mission," *Publications of the Astronomical Society of the Pacific*, vol. 135, p. 068001, June 2023, doi: 10.1088/1538-3873/acd1b5.

[2] A. G. Adame *et al.*, "DESI 2024 VI: cosmological constraints from the measurements of baryon acoustic oscillations," *Journal of Cosmology and Astroparticle Physics*, vol. 2025, no. 02, p. 021, Feb. 2025, doi: 10.1088/1475-7516/2025/02/021.

[3] M. Boylan-Kolchin, "Stress testing ΛCDM with high-redshift galaxy candidates," *Nature Astronomy*, vol. 7, no. 6, pp. 731–735, June 2023, doi: 10.1038/s41550-023-01937-7.

[4] R. P. Naidu *et al.*, "Two Remarkably Luminous Galaxy Candidates at z ≈ 10-12 Revealed by JWST," *The Astrophysical Journal*, vol. 940, p. L14, Nov. 2022, doi: 10.3847/2041-8213/ac9b22.

[5] K. Kreckel *et al.*, "The Void Galaxy Survey: Optical Properties and H I Morphology and Kinematics," *The Astronomical Journal*, vol. 144, p. 16, July 2012, doi: 10.1088/0004-6256/144/1/16.

[6] S. E. Nuza, F.-S. Kitaura, S. Heß, N. I. Libeskind, and V. Müller, "The cosmic web of the Local Universe: cosmic variance, matter content and its relation to galaxy morphology," *Monthly Notices of the Royal Astronomical Society*, vol. 445, no. 1, pp. 988–1001, Nov. 2014, doi: 10.1093/mnras/stu1746.

[7] N. I. Libeskind *et al.*, "Tracing the cosmic web," *Monthly Notices of the Royal Astronomical Society*, vol. 473, no. 1, pp. 1195–1217, Jan. 2018, doi: 10.1093/mnras/stx1976.

[8] R. Sakidja, "The Curvature–Transport Correspondence (CTC): From Quantum Effective Mass to Cosmological Dark Matter." Zenodo, Dec. 2025. doi: 10.5281/zenodo.17805651.

[9] R. M. Wald, *General Relativity*. Chicago, USA: Chicago Univ. Pr., 1984. doi: 10.7208/chicago/9780226870373.001.0001.

[10] J. R. Bond, L. Kofman, and D. Pogosyan, "How filaments of galaxies are woven into the cosmic web," *Nature*, vol. 380, no. 6575, pp. 603–606, Apr. 1996, doi: 10.1038/380603a0.

[11] R. van de Weygaert and E. Platen, "Cosmic Voids: Structure, Dynamics and Galaxies," *Int. J. Mod. Phys. Conf. Ser.*, vol. 01, pp. 41–66, Jan. 2011, doi: 10.1142/S2010194511000092.

[12] R. B. Tully, H. Courtois, Y. Hoffman, and D. Pomarède, "The Laniakea supercluster of galaxies," *Nature*, vol. 513, no. 7516, pp. 71–73, Sept. 2014, doi: 10.1038/nature13674.

[13] M. A. Aragón-Calvo, R. van de Weygaert, and B. J. T. Jones, "Multiscale phenomenology of the cosmic web," *Monthly Notices of the Royal Astronomical Society*, vol. 408, no. 4, pp. 2163–2187, Nov. 2010, doi: 10.1111/j.1365-2966.2010.17263.x.

[14] I. Labbé *et al.*, "A population of red candidate massive galaxies ~600 Myr after the Big Bang," *Nature*, vol. 616, no. 7956, pp. 266–269, Apr. 2023, doi: 10.1038/s41586-023-05786-2.

[15] M. Haslbauer, I. Banik, and P. Kroupa, "The KBC void and Hubble tension contradict ΛCDM on a Gpc scale − Milgromian dynamics as a possible solution," *Monthly Notices of the Royal*

Astronomical Society, vol. 499, no. 2, pp. 2845–2883, Oct. 2020, doi: 10.1093/mnras/staa2348.
[16] J. R. Gott III *et al.*, “A Map of the Universe,” *The Astrophysical Journal*, vol. 624, no. 2, p. 463, May 2005, doi: 10.1086/428890.
[17] I. Horváth, Z. Bagoly, J. Hakkila, and L. V. Tóth, “New data support the existence of the Hercules-Corona Borealis Great Wall⋆,” *A&A*, vol. 584, Dec. 2015, doi: 10.1051/0004-6361/201424829.
[18] E. Di Valentino *et al.*, “In the realm of the Hubble tension—a review of solutions,” *Classical and Quantum Gravity*, vol. 38, no. 15, p. 153001, July 2021, doi: 10.1088/1361-6382/ac086d.
[19] C. Krishnan, R. Mohayaee, E. Ó. Colgáin, M. M. Sheikh-Jabbari, and L. Yin, “Hints of FLRW breakdown from supernovae,” *Phys. Rev. D*, vol. 105, no. 6, p. 063514, Mar. 2022, doi: 10.1103/PhysRevD.105.063514.
[20] L. D. Landau and E. M. Lifshitz, *Theory of Elasticity*, vol. 7. in Course of Theoretical Physics, vol. 7. New York: Elsevier Butterworth-Heinemann, 1986. doi: 10.1016/C2009-0-25521-8.
[21] C. Kittel and P. McEuen, *Introduction to Solid State Physics*. Wiley, 2018. [Online]. Available: https://books.google.com/books?id=nNpVEAAAQBAJ
[22] J. Crank, *The Mathematics of Diffusion*. in Oxford science publications. Clarendon Press, 1979. [Online]. Available: https://books.google.com/books?id=eHANhZwVouYC
[23] S. Sachdev, *Quantum Phase Transitions*. Cambridge University Press, 2011. doi: 10.1017/cbo9780511973765.
[24] Planck Collaboration *et al.*, “Planck 2018 results,” *A&A*, vol. 641, 2020, doi: 10.1051/0004-6361/201833910.
[25] C. Franco and others, “The homogeneity scale in the Local Universe: model-independent estimate from S-PLUS DR4 blue galaxies,” Nov. 2025.
[26] P. Sarkar, J. Yadav, B. Pandey, and S. Bharadwaj, “The scale of homogeneity of the galaxy distribution in SDSS DR6,” *Monthly Notices of the Royal Astronomical Society: Letters*, vol. 399, no. 1, pp. L128–L131, Oct. 2009, doi: 10.1111/j.1745-3933.2009.00738.x.
[27] M. C. Cross and P. C. Hohenberg, “Pattern formation outside of equilibrium,” *Rev. Mod. Phys.*, vol. 65, no. 3, pp. 851–1112, July 1993, doi: 10.1103/RevModPhys.65.851.
[28] Y.-C. Chen *et al.*, “Detecting galaxy–filament alignments in the Sloan Digital Sky Survey III,” *Monthly Notices of the Royal Astronomical Society*, vol. 485, no. 2, pp. 2492–2504, May 2019, doi: 10.1093/mnras/stz539.
[29] S. Tavasoli and P. Ghafour, “The Filament Rift: ΛCDM’s Structural Challenge against Observation,” *The Astrophysical Journal*, vol. 994, no. 2, p. 219, Nov. 2025, doi: 10.3847/1538-4357/ae18d6.
[30] DES Collaboration *et al.*, “Dark energy survey year 3 results: Cosmological constraints from cluster abundances, weak lensing, and galaxy clustering,” *Phys. Rev. D*, vol. 112, no. 8, p. 083535, Oct. 2025, doi: 10.1103/3dzh-d8f5.
[31] A. Rollett, F. J. Humphreys, G. S. Rohrer, and M. Hatherly, *Recrystallization and Related Annealing Phenomena*. Pergamon, 2004. [Online]. Available: https://books.google.com/books?id=52Gloa7HxGsC
[32] J. W. Cahn, “On spinodal decomposition,” *Acta Metallurgica*, vol. 9, no. 9, pp. 795–801, Sept. 1961, doi: 10.1016/0001-6160(61)90182-1.

[33] E. Tarleton, “Dislocations, Mesoscale Simulations and Plastic Flow, Oxford Series on Materials Modelling 5, by Ladislas Kubin,” *Contemporary Physics*, vol. 54, no. 6, pp. 302–303, Nov. 2013, doi: 10.1080/00107514.2013.856946.
[34] S. W. Hawking and G. F. R. Ellis, *The Large Scale Structure of Space-Time*. in Cambridge Monographs on Mathematical Physics. Cambridge University Press, 2023. doi: 10.1017/9781009253161.
[35] R. Penrose, “Gravitational Collapse and Space-Time Singularities,” *Phys. Rev. Lett.*, vol. 14, no. 3, pp. 57–59, Jan. 1965, doi: 10.1103/PhysRevLett.14.57.
[36] S. M. Sze and K. K. Ng, *Physics of Semiconductor Devices*. Wiley, 2006. [Online]. Available: https://books.google.com/books?id=o4unkmHBHb8C
[37] D. Hull and D. J. Bacon, *Introduction to Dislocations*. Butterworth-Heinemann, 2001. [Online]. Available: https://books.google.com/books?id=EHjrGd-4TLcC
[38] C. W. Misner, K. S. Thorne, J. A. Wheeler, and D. I. Kaiser, *Gravitation*. Princeton University Press, 2017. [Online]. Available: https://books.google.com/books?id=SyQzDwAAQBAJ
[39] M. Maggiore, *Gravitational Waves: Volume 1: Theory and Experiments*. 2007. doi: 10.1093/acprof:oso/9780198570745.001.0001.
[40] F. G. Friedlander, *The Wave Equation on a Curved Space-Time*. Cambridge University Press, 1975. [Online]. Available: https://books.google.com/books?id=RDmpajLTw1oC
[41] C. Bär, N. Ginoux, and F. Pfäffle, *Wave Equations on Lorentzian Manifolds and Quantization*. in ESI lectures in mathematics and physics. European Mathematical Society, 2007. [Online]. Available: https://books.google.com/books?id=nzi-c0dP1NYC
[42] H. Ringström, *The Cauchy Problem in General Relativity*. in ESI lectures in mathematics and physics. European Mathematical Society, 2009. [Online]. Available: https://books.google.com/books?id=dFPuLLvzWYwC
[43] J. Bardeen, “Nonsingular general relativistic gravitational collapse”.
[44] I. Dymnikova, “Vacuum nonsingular black hole,” *General Relativity and Gravitation*, vol. 24, no. 3, pp. 235–242, Mar. 1992, doi: 10.1007/BF00760226.
[45] S. A. Hayward, “Formation and Evaporation of Nonsingular Black Holes,” *Phys. Rev. Lett.*, vol. 96, no. 3, p. 031103, Jan. 2006, doi: 10.1103/PhysRevLett.96.031103.
[46] V. P. Frolov, “Notes on nonsingular models of black holes,” *Phys. Rev. D*, vol. 94, no. 10, p. 104056, Nov. 2016, doi: 10.1103/PhysRevD.94.104056.
[47] M. A. Markov, “Limiting density of matter as a universal law of nature,” *ZhETF Pisma Redaktsiiu*, vol. 36, pp. 214–216, Sept. 1982.
[48] V. P. Frolov, M. A. Markov, and V. F. Mukhanov, “Black holes as possible sources of closed and semiclosed worlds,” *Phys. Rev. D*, vol. 41, no. 2, pp. 383–394, Jan. 1990, doi: 10.1103/PhysRevD.41.383.
[49] K. Skenderis and M. Taylor, “The fuzzball proposal for black holes,” *Physics Reports*, vol. 467, no. 4, pp. 117–171, Oct. 2008, doi: 10.1016/j.physrep.2008.08.001.
[50] D. R. Tilley and J. Tilley, *Superfluidity and Superconductivity*. in Graduate Student Series in Physics. Taylor & Francis, 1990. [Online]. Available: https://books.google.com/books?id=I6JtWd3J8MIC
[51] F. J. RICHARDS, “A Flexible Growth Function for Empirical Use,” *Journal of Experimental Botany*, vol. 10, no. 2, pp. 290–301, June 1959, doi: 10.1093/jxb/10.2.290.

[52] U. F. Kocks and H. Mecking, “Physics and phenomenology of strain hardening: the FCC case,” *Progress in Materials Science*, vol. 48, no. 3, pp. 171–273, Jan. 2003, doi: 10.1016/S0079-6425(02)00003-8.
[53] W. Shockley and W. T. Read, “Statistics of the Recombinations of Holes and Electrons,” *Phys. Rev.*, vol. 87, no. 5, pp. 835–842, Sept. 1952, doi: 10.1103/PhysRev.87.835.
[54] W. Fiszdon, “Quantized Vortices in Helium II. By R. J. DONNELLY. Cambridge University Press, 1991. 346 pp. £95.,” *Journal of Fluid Mechanics*, vol. 233, pp. 691–692, 1991, doi: 10.1017/S0022112091220650.
[55] L. A. Dissado and J. C. Fothergill, *Electrical Degradation and Breakdown in Polymers*. in IEE materials & devices series. P. Peregrinus, 1992. [Online]. Available: https://books.google.com/books?id=8Tm7dH99-XEC
[56] S. Corbel, M. A. Nowak, R. P. Fender, A. K. Tzioumis, and S. Markoff, “Radio/X-ray correlation in the low/hard state of GX 339–4,” *A&A*, vol. 400, no. 3, pp. 1007–1012, 2003, doi: 10.1051/0004-6361:20030090.
[57] S. Corbel *et al.*, “The ‘universal’ radio/X-ray flux correlation: the case study of the black hole GX 339−4,” *Monthly Notices of the Royal Astronomical Society*, vol. 428, no. 3, pp. 2500–2515, Jan. 2013, doi: 10.1093/mnras/sts215.
[58] A. Merloni, S. Heinz, and T. Di Matteo, “A Fundamental Plane of black hole activity,” *Mon Not R Astron Soc*, vol. 345, no. 4, pp. 1057–1076, 2003, doi: 10.1046/j.1365-2966.2003.07017.x.
[59] R. M. Plotkin, S. F. Anderson, W. N. Brandt, S. Markoff, O. Shemmer, and J. Wu, “THE LACK OF TORUS EMISSION FROM BL LACERTAE OBJECTS: AN INFRARED VIEW OF UNIFICATION WITH WISE,” *The Astrophysical Journal Letters*, vol. 745, no. 2, p. L27, Jan. 2012, doi: 10.1088/2041-8205/745/2/L27.
[60] F. Yuan and R. Narayan, “Hot Accretion Flows Around Black Holes,” *Annual Review of Astronomy and Astrophysics*, vol. 52, no. Volume 52, 2014. Annual Reviews, pp. 529–588, 2014. doi: https://doi.org/10.1146/annurev-astro-082812-141003.
[61] J. S. Bloom *et al.*, “A Possible Relativistic Jetted Outburst from a Massive Black Hole Fed by a Tidally Disrupted Star,” *Science*, vol. 333, no. 6039, pp. 203–206, July 2011, doi: 10.1126/science.1207150.
[62] B. A. Zauderer *et al.*, “Birth of a relativistic outflow in the unusual γ-ray transient Swift J164449.3+573451,” *Nature*, vol. 476, no. 7361, pp. 425–428, Aug. 2011, doi: 10.1038/nature10366.
[63] F. Wilczek, “QCD and Natural Philosophy,” *Annales Henri Poincaré*, vol. 4, pp. 211–228, Dec. 2003, doi: 10.1007/s00023-003-0917-y.
[64] G. F. Giudice, “Naturally Speaking: The Naturalness Criterion and Physics at the LHC,” pp. 155–178, Jan. 2008, doi: 10.1142/9789812779762_0010.
[65] G. Aad *et al.*, “Observation of a new particle in the search for the Standard Model Higgs boson with the ATLAS detector at the LHC,” *Physics Letters B*, vol. 716, no. 1, pp. 1–29, Sept. 2012, doi: 10.1016/j.physletb.2012.08.020.
[66] L. Susskind, “Dynamics of spontaneous symmetry breaking in the Weinberg-Salam theory,” *Phys. Rev. D*, vol. 20, no. 10, pp. 2619–2625, Nov. 1979, doi: 10.1103/PhysRevD.20.2619.
[67] S. P. Martin, “A Supersymmetry primer,” *Adv. Ser. Direct. High Energy Phys.*, vol. 18, pp. 1–98, 1998, doi: 10.1142/9789812839657_0001.

[68] S. Weinberg, “What is Quantum Field Theory, and What Did We Think It Is?,” *arXiv e-prints*, p. hep-th/9702027, Feb. 1997, doi: 10.48550/arXiv.hep-th/9702027.
[69] C. Patrignani, “Review of Particle Physics,” *Chinese Physics C*, vol. 40, no. 10, p. 100001, Oct. 2016, doi: 10.1088/1674-1137/40/10/100001.
[70] F. Englert and R. Brout, “Broken Symmetry and the Mass of Gauge Vector Mesons,” *Phys. Rev. Lett.*, vol. 13, no. 9, pp. 321–323, Aug. 1964, doi: 10.1103/PhysRevLett.13.321.
[71] F. Wilczek, “Asymptotic freedom: From paradox to paradigm,” *Proc. Nat. Acad. Sci.*, vol. 102, pp. 8403–8413, 2005, doi: 10.1103/RevModPhys.77.857.
[72] N. W. Ashcroft and N. D. Mermin, *Solid State Physics*. in HRW international editions. Holt, Rinehart and Winston, 1976. [Online]. Available: https://books.google.com/books?id=1C9HAQAAIAAJ
[73] N. Goldenfeld, *Lectures on phase transitions and the renormalization group*. 1992.
[74] E. Abrahams, P. W. Anderson, D. C. Licciardello, and T. V. Ramakrishnan, “Scaling Theory of Localization: Absence of Quantum Diffusion in Two Dimensions,” *Phys. Rev. Lett.*, vol. 42, no. 10, pp. 673–676, Mar. 1979, doi: 10.1103/PhysRevLett.42.673.
[75] J. D. Bekenstein, “Black Holes and Entropy,” *Phys. Rev. D*, vol. 7, no. 8, pp. 2333–2346, Apr. 1973, doi: 10.1103/PhysRevD.7.2333.
[76] S. W. Hawking, “Particle creation by black holes,” *Communications in Mathematical Physics*, vol. 43, no. 3, pp. 199–220, Aug. 1975, doi: 10.1007/BF02345020.
[77] A. J. Liu and S. R. Nagel, “The Jamming Transition and the Marginally Jammed Solid,” *Annual Review of Condensed Matter Physics*, vol. 1, no. Volume 1, 2010. Annual Reviews, pp. 347–369, 2010. doi: https://doi.org/10.1146/annurev-conmatphys-070909-104045.
[78] C. A. Angell, “Formation of Glasses from Liquids and Biopolymers,” *Science*, vol. 267, no. 5206, pp. 1924–1935, Mar. 1995, doi: 10.1126/science.267.5206.1924.
[79] R. B. Bird, *Dynamics of Polymeric Liquids, Volume 1: Fluid Mechanics*. in Dynamics of Polymeric Liquids. Wiley, 1987. [Online]. Available: https://books.google.com/books?id=posvAQAAIAAJ
[80] J. D. Ferry, *Viscoelastic Properties of Polymers*. Wiley, 1980. [Online]. Available: https://books.google.com/books?id=9dqQY3Ujsx4C
[81] M. Rubinstein and R. H. Colby, *Polymer Physics*. OUP Oxford, 2003. [Online]. Available: https://books.google.com/books?id=RHksknEQYsYC
[82] P. G. de Gennes, *Scaling Concepts in Polymer Physics*. Cornell University Press, 1979. [Online]. Available: https://books.google.com/books?id=Gh1TcAAACAAJ
[83] M. Doi and S. F. Edwards, *The theory of polymer dynamics*. in International series of monographs on physics. Oxford: Oxford Univ. Press, 1986. [Online]. Available: https://cds.cern.ch/record/346518
[84] P. M. Chaikin and T. C. Lubensky, *Principles of Condensed Matter Physics*. Cambridge University Press, 2000. [Online]. Available: https://books.google.com/books?id=P9YjNjzr9OIC

SUPPLEMENT S1. Numerical Demonstration of Curvature Saturation in the CTC Framework

This supplement documents the numerical procedures used to generate the four illustrative figures accompanying Section 3 of the main text.

All simulations were performed using the Jupyter notebook *ctc_black_hole_saturation.ipynb* available in https://github.com/sakidja/CTC_related_papers/, which provides a transparent, reproducible implementation of the Curvature–Transport Correspondence (CTC) in a simplified radial model.

Unless otherwise stated, all simulations use a reference mass

$$M_{\mathrm{ref}} = 10\, M_{\odot}. \qquad \text{(S1-1)}$$

S1.1. Classical Curvature Baseline

The notebook computes the Schwarzschild Kretschmann invariant,

$$K_{\mathrm{GR}}(r) = \frac{48G^2M^2}{c^4r^6}, \qquad \text{(S1-2)}$$

as the unregularized curvature profile predicted by general relativity.
This divergent expression forms the baseline against which the CTC-saturated curvature profile is compared.

S1.2. Saturation Condition and Core Radius

CTC replaces the classical divergence by imposing a finite maximum curvature K_{max}.
The *saturated core radius* is computed from

$$K_{\mathrm{GR}}(r_s) = K_{\mathrm{max}}, r_s(M) = \left(\frac{48G^2M^2}{c^4K_{\mathrm{max}}}\right)^{1/6}. \qquad \text{(S1-3)}$$

This relation determines the location of the CTC interior phase.

S1.3. Figure S1 — Curvature Profile at the Reference Mass

Generated using: plot_curvature_profiles() with default input $M = M_{\mathrm{ref}}$.
Figure S1 shows:

- the classical Schwarzschild curvature (solid blue),
- the CTC-saturated curvature (dashed orange),
- the saturated core radius $r_s(M_{\mathrm{ref}})$(dotted line).

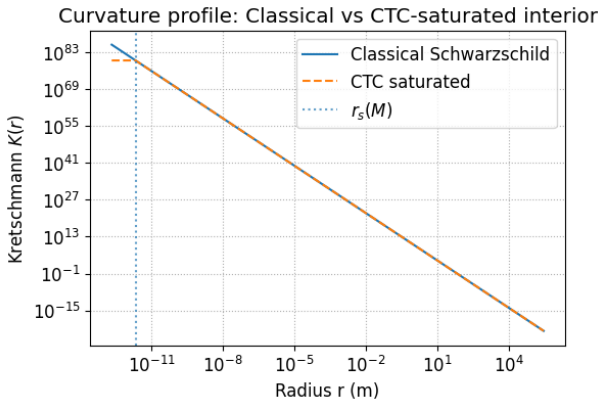

This figure establishes the finite-curvature interior predicted by the CTC model.

S1.4. Figure S2 — Mass Scaling of the Saturated Core

Generated using: scan_core_radius() over a mass range $1–100\ M_{\odot}$.

Figure S2 shows:

- the monotonic expansion of the saturated core radius with mass,
- consistent scaling $r_s(M) \propto M^{1/3}$,
- confirmation that curvature remains fixed while the interior region grows.

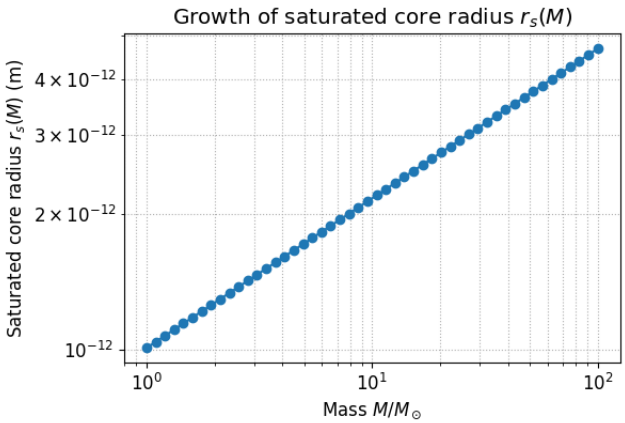

Although the figure spans many masses, the reference mass M_{ref} remains the same mass chosen for the main text.

S1.5. Figure S3 — Hypothetical Curvature Profile at an Alternative Mass

Generated either by:

- calling plot_curvature_profiles manually with a different value of M, or using the interactive slider provided in Cell 7 of the notebook.
- This figure is not tied to the reference mass. It illustrates how the curvature plateau and core radius shift for other hypothetical black hole masses.

The function of this figure is pedagogical:

- it shows the generality of the CTC mechanism,
- it confirms that the shape of the curvature profile is robust under changes in M,
- it links analytic predictions to numerical behavior.

Because the mass is user-selected, the figure is best described as a hypothetical example, not a reference calculation.

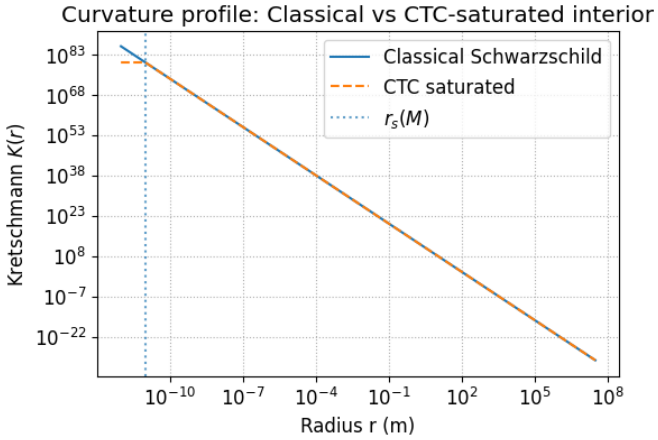

S1.6. Figure S4 — Flux Divergence Saturation at the Reference Mass

Generated using:
plot_divergence_profile() with default $M = M_{\mathrm{ref}}$.

This figure displays a toy model of the divergence field $\nabla \cdot F_G(r)$with:

- a classical-like exterior profile,
- a sharp downturn near $r_s(M_{\mathrm{ref}})$,
- saturation at $-D_{\mathrm{max}}$inside the core.

The location of the transition reflects the reference mass; the qualitative shape illustrates the essential ingredient of CTC: collapse is limited by *transport capacity*, not by unbounded compression.

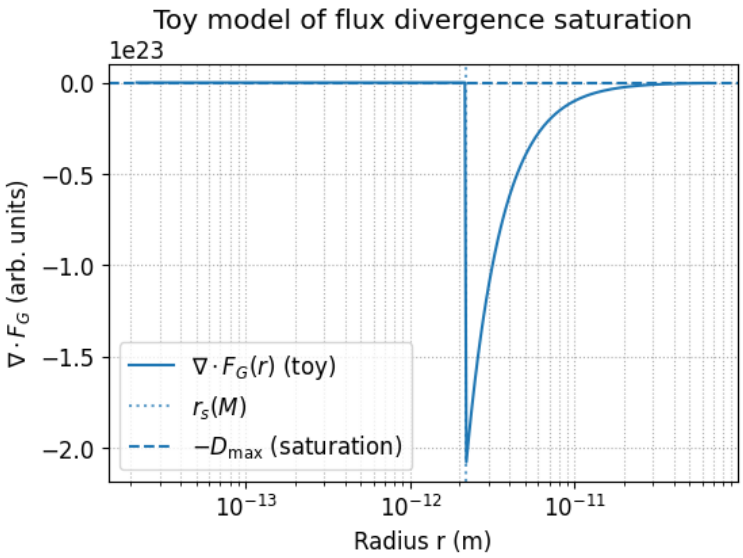

SUPPLEMENT S2 Correspondence with Materials Science and Transport Theory

A central ingredient of the Curvature Transport Correspondence is the scale dependence of the vacuum stiffness $\kappa(E)$, governed by

$$\frac{d\kappa(E)}{dE} = -\frac{\kappa(E)}{\gamma(E)}. \qquad \text{(S2-1)}$$

This differential structure is not unique to gravitational transport. Equations of precisely this form arise throughout materials science, condensed matter physics, and statistical transport theory whenever a response coefficient varies because underlying microstates reorganize across scale, frequency, or energy. The generic form is

$$\frac{dC}{d\lambda} = -\frac{C}{\Gamma(\lambda)}, \qquad \text{(S2-2)}$$

where C is a modulus or transport coefficient, λ is a control parameter, and $\Gamma(\lambda)$ is a susceptibility that encodes how easily the microscopic structure redistributes flux, stress, or momentum. The mapping

$$C \to \kappa, \lambda \to E, \Gamma \to \gamma$$

shows that (S3-1) is mathematically identical to the standard renormalization law (S2-2).

Below we summarize representative examples.

S2.1. Elastic moduli under microstructural renormalization

Landau and Lifshitz demonstrate that elastic constants in heterogeneous solids acquire scale dependence through coarse graining (Landau and Lifshitz, *Theory of Elasticity*)[20]. The bulk modulus satisfies

$$\frac{dK}{dl} = -\frac{K}{\Gamma(l)}, \qquad \text{(S2-3)}$$

where l is a coarse graining scale and $\Gamma(l)$reflects microstructural susceptibility.
Equation (S3) has the same structure as the CTC stiffness flow (S1).

S2.2. Scale dependent conductivity in disordered systems (Abrahams–Anderson–Licciardello–Ramakrishnan)

A structurally identical renormalization equation governs the conductivity in disordered conductors.
In their seminal work, Abrahams, Anderson, Licciardello, and Ramakrishnan[74] established the scaling theory of localization and showed that the conductivity σ satisfies

$$\frac{d\sigma}{d\ln\, L} = -\frac{\sigma}{\beta(\sigma)}, \qquad \text{(S2-4)}$$

where L is the running length scale and $\beta(\sigma)$ acts as an inverse susceptibility that determines how the system responds to coarse-graining. Rewriting (S4):

$$\frac{d\sigma}{dL} = -\frac{\sigma}{L\,\beta(\sigma)}, \qquad \text{(S2-5)}$$

reveals that $\sigma(L)$ obeys the same inverse-susceptibility evolution as (S3-2), and hence as the stiffness flow (S3-1). This is a direct analogue of the CTC relation, with

$$C = \sigma, \qquad \lambda = L, \qquad \Gamma = L\beta(\sigma).$$

S2.3. Effective mass renormalization in crystalline solids

In many-body treatments, the electron effective mass satisfies

$$\frac{dm^*}{d\omega} = -\frac{m^*}{\Sigma'(\omega)}, \qquad \text{(S2-6)}$$

where $\Sigma'(\omega)$ is the derivative of the electronic self-energy (Ashcroft and Mermin, *Solid State Physics*)[72]. This is another direct realization of the structure (S2): the response coefficient m^* runs with energy because the underlying microstates reorganize.

S2.4. Viscoelastic Relaxation and Frequency-Dependent Stiffness

In viscoelastic materials the shear modulus $G(\omega)$ depends on the driving frequency ω, and its evolution is controlled by a relaxation spectrum. Classical rheology [79], [80], [81] shows that the modulus satisfies differential relations of the form

$$\frac{dG}{d\omega} = -\frac{G}{\omega\,\tau(\omega)}, \qquad \text{(S2-7)}$$

where $\tau(\omega)$ is a relaxation susceptibility encoding how rapidly the material can reorganize microstructurally. Equation (S7) has the same structural form as the CTC flow equation (S1): a response coefficient evolves according to its inverse susceptibility. This reinforces that the CTC relation is a familiar renormalization structure found in well-established viscoelastic theory.

S2.5. Polymer Networks and Soft-Matter Systems

Scaling theories of polymer networks and soft matter [82], [83], [84] that the effective stiffness $K(\lambda)$ changes under coarse-graining or deformation by a renormalization equation of the form

$$\frac{dK}{d\ln\,\lambda} = -\frac{K}{S(\lambda)}, \qquad \text{(S2-8)}$$

where $S(\lambda)$is the structural susceptibility of the network. Here again, the logarithmic derivative of the modulus is controlled by the inverse susceptibility—exactly matching the CTC structure in (S1). Polymer networks therefore provide another concrete example where stiffness evolves through a transport-mediated reorganization of microstructure, directly analogous to the running vacuum stiffness $\kappa(E)$in the CTC framework.

S.2.6. Summary

Equation (S1), central to the Curvature Transport Correspondence, is not a new or exotic structure. It is the gravitational analogue of the universal renormalization law (S2) appearing throughout condensed matter and materials science:

Whenever a response coefficient depends on microstate organization, its logarithmic derivative is controlled by an inverse susceptibility.

Thus the scale evolution of vacuum stiffness in the CTC follows a well-established physical mechanism: transport mediated response coefficients necessarily run with scale.